

Load sequence effects and cyclic deformation behaviour of 7075-T651 aluminium alloy

R. Branco[a,1], J.D. Costa[a], P.A. Prates[b,a], F. Berto[c], C. Pereira[d], A. Mateus[d]

[a] University of Coimbra, CEMMPRE, Department of Mechanical Engineering, Coimbra, Portugal

[b] Department of Mechanical Engineering, Centre for Mechanical Technology & Automation (TEMA), University of Aveiro, 3810-193 Aveiro, Portugal

[c] Department of Mechanical and Industrial Engineering, NTNU, 7491 Trondheim, Norway

[d] Centre for Rapid and Sustainable Product Development, Polytechnic Institute of Leiria, Rua de Portugal, Marinha Grande, 2430-028, Portugal

Abstract

This paper investigates the effect of loading history on cyclic deformation and fatigue behaviour of 7075-T651 aluminium alloy subjected to two-step loading. High-low and low-high sequences, encompassing both symmetrical and asymmetrical steps, are performed under strain-controlled mode for different loading scenarios. An elastic-plastic constitutive model is developed using the finite element method to simulate the stabilised stress-strain response. Fatigue life predictions are made by applying strain-based, energy-based, and SWT-based methods. The SWT-based model properly captured the effect of load history on fatigue behaviour. In addition, fatigue life predictions carried out using the numerical simulations agreed well with the experiments.

Keywords: load sequence; variable-amplitude loading; step loading; cumulative damage; linear damage rule; cyclic deformation; 7075-T651 aluminium alloy.

1. Introduction

Aluminium alloys have a major application in aviation, aerospace, and automotive industries due to their low density, high strength, good fracture toughness, and attractive cost [1-2]. In these areas of application, most components are exposed to variable-amplitude loading which makes them prone to fatigue failure [3-4]. On the other hand, although fatigue design often assumes that materials are loaded in the elastic range, at the critical geometric discontinuities, local plastic deformation can occur [5-7]. Therefore, the development of robust engineering

[1] Corresponding author: R. Branco (ricardo.branco@dem.uc.pt)

design methods against fatigue requires not only the knowledge of the loading history but also an adequate understating of the cyclic deformation behaviour.

Material response to cyclic deformation (e.g. cyclic hardening, cyclic softening, mean stress relaxation, ratcheting) is not a trivial problem, because it is history dependent, i.e. the cyclic stress-strain response may significantly change with the load sequence [8-9]. It is also well-known that cyclic deformation response is material dependent [10-12]. Particularly in the case of aluminium alloys, because of they have face-centred cubic crystal structures with high stacking fault energy, their cyclic deformation response is less dependent on the loading history than that of other engineering materials, namely face-centred cubic metals with low stacking fault energy, which can be advantageous regarding the development of reliable fatigue design methods.

Another important aspect, not negligible, in fatigue design is the mean stress effect. Several attempts have been made in the past to account for such a phenomenon. Regarding precipitation-hardening aluminium alloys, literature shows that positive mean stresses are detrimental to fatigue life, while negative mean stresses are beneficial, and that mean stress relaxation rates depend on strain ratio, strain amplitude, and material type [13-14]. In addition, under strain-controlled conditions, when there is full relaxation of mean stress, fatigue life is not significantly affected. It is also known that cyclic softening materials, such as high-strength aluminium alloys, are more susceptible to mean stress relaxation than cyclic hardening materials [15].

In a design point of view, fatigue life assessment under variable-amplitude loading requires an accurate calculation of damage accumulation. Cumulative fatigue damage theories have attracted much attention overt the last decades [16-17]. Although there are many approaches available in the literature, the most commonly used, partly due to its simplicity, is the so-called Palmgren-Miner rule, which assumes that damage is accumulated linearly [18]. Its most obvious shortcoming is the inability to deal with load sequence effects. Due to the triangular relationship between load sequence, damage accumulation, and fatigue life, such effects cannot be ignored. A comprehensive discussion about the most relevant theories to deal with load interaction effects can be found in the papers by Zhu et al. [19,20].

So far, very few studies have addressed the effect of loading sequence on fatigue life in aluminium alloys subjected to uniaxial strain-controlled conditions [21-24]. Colin an Fatemi

[18] concluded that a fatigue model based on the Smith-Watson-Topper (SWT) parameter in conjunction with a linear damage rule can capture the load sequence effect. When compared to the commonly used methods that combine the above-mentioned damage rule with conventional stress-life or strain-life relationships, the fatigue life predictions were considerably better. This improvement was attributed to the fact that the SWT parameter includes both stress and strain terms, making it more suitable for deformation-sensitive materials. Additionally, it is able to account for mean stress effects [25].

Experimental analysis of load sequence effects on cyclic deformation behaviour and fatigue life, particularly for realistic geometries and in-service loading spectra, is expensive and time-consuming. With the advent of computer technology, numerical methods can be advantageously introduced to develop precise cyclic constitutive models, allowing the simulation of different load histories quickly and cheaply [26-27]. Regarding the 7075-aluminium alloy, limited work has been published on cyclic constitutive models. Two exceptions are the recent papers by Agius et al. [26] and Nath et al. [27]. However, the focus has been put on hysteresis loop development; the effect of loading history on the fatigue life has not been addressed.

The present paper aims to study the load sequence effect on both the cyclic plastic behaviour and the fatigue life in the 7075-T651 aluminium alloy under two-step loading. Firstly, experimental tests encompassing both high-low and low-high sequences are performed for the studied material under strain-controlled mode. Then, an elastic-plastic model is developed from fully-reversed constant-amplitude data to simulate the stabilised stress-strain response. Finally, fatigue life predictions are performed using strain-based, energy-based, and SWT-based methods and the damage accumulation is accounted for with a linear damage rule.

2. Material and methods

The material studied in this research was the 7075-T651 aluminium alloy supplied in the form of a 35mm-thick plate. Its nominal chemical composition and its main monotonic tensile properties are listed in Table 1 and Table 2, respectively. Two types of cylindrical specimens, machined according to ASTM E606 standard, were tested: one with a 19mm-long and 6mm-diameter gauge section, and another with a 15mm-long and 8mm-diameter gauge section. In order to prevent buckling problems, the former was used for lower strain amplitudes, while the latter was used for higher strain amplitudes.

The tests were carried out at room temperature under uniaxial strain-control mode using sinusoidal waves and a constant strain rate (8×10^{-3} s^{-1}). Failure was defined as 40% load drop from the first cycle, or fracture, whichever occurred first. The cyclic stress-strain response was recorded using a 12.5mm-long mechanical extensometer clamped directly to the gauge section of the specimen. Silicon carbide paper of different grades (P600-grit, P1200-grit, and P2500-grit) and 3-µm alumina-based polishing compound were used to reduce the effect of surface roughness on fatigue life.

Three cyclic strain histories (see Fig. 1) were study: constant-amplitude, high-low sequences, and low-high sequences. The constant-amplitude tests were conducted under fully-reversed conditions with strain amplitudes between 0.5% and 2.75% (see Table 3). The high-low and low-high sequences included two steps of constant amplitude loading with a fix maximum strain. The higher step was symmetrical (i.e. $R_\varepsilon = -1$) while the other was asymmetrical (i.e. $R_\varepsilon \neq -1$). The first step was applied for a limited number of cycles (n_1) defined as 20% of the total fatigue life of the constant-amplitude loading case carried out at the same strain amplitude (see Table 3).

3. Numerical modelling and simulation

The simulation of cyclic plastic behaviour of the 7075-T651 aluminium alloy was done using a constitutive model based on the von Mises yield criterion coupled with a mixed isotropic-kinematic hardening law under an associated flow rule, as follows:

$$f(\sigma' - X) - Y \leq 0 \tag{1}$$

where $f(\sigma' - X)$ represents the von Mises yield criterion, σ' is the deviatoric Cauchy stress tensor, X is the backstress tensor (described by a non-linear kinematic hardening law) and Y is the yield stress (described by the isotropic hardening law). For the aluminium alloy, the yield stress was modelled using a Voce isotropic hardening law, i.e.

$$Y = Y_0 + (Y_{sat} - Y_0)[1 - \exp(-C_Y \bar{\varepsilon}^p)] \tag{2}$$

where Y_0, Y_{sat}, and C_Y are material parameters and $\bar{\varepsilon}^p$ is the equivalent plastic strain.

The non-linear kinematic hardening was modelled via an Armstrong-Frederick law:

$$\dot{X} = C_X \left[\frac{X_{sat}}{\overline{\sigma}} (\sigma' - X) - X \right] \dot{\overline{\varepsilon}}^p \quad (3)$$

where $\dot{X}$ is the backstress rate, C_X, and X_{sat} are material parameters, $\overline{\sigma}$ is the equivalent stress, and $\dot{\overline{\varepsilon}}^p$ is the equivalent plastic strain rate. The determination of the material constants that best described the cyclic elastic-plastic behaviour of both steels was carried out by minimising the function:

$$F(A) = \sum_{i=1}^{N} \left(\frac{\sigma^{Num}(A) - \sigma^{Exp}}{\sigma^{Exp}} \right)_i^2 \quad (4)$$

where $\sigma^{Num}(A)$ and σ^{Exp} are the analytical fitted and the experimentally measured values of true stress at point i (which corresponds to a given equivalent plastic strain value), N is the total number of experimental data points, and A is the set of material parameters to be identified. The fitting procedure was conducted using the data collected in the constant-amplitude loading tests for the different strain amplitudes (see Table 3) by applying a non-linear gradient-based optimisation algorithm [28].

The finite element model used to simulate the saturated cyclic stress-strain behaviour of the tested alloy under strain-control mode consisted of a single 8-node three-dimensional isoparametric finite element (see Figure 2). Simulations were performed with the DD3IMP, an implicit three-dimensional finite element code developed at the University of Coimbra for the analysis of sheet metal forming processes [29]. The cyclic loads were applied in four nodes located in the plane x = 1 mm along the direction parallel to the x-axis assuming 200 load sub-steps per cycle. Symmetry conditions were imposed in the planes x=0, y=0 and z=0.

Figure 3 compares the cyclic stress-strain response obtained in the experiments with that simulated numerically for a strain amplitude (ε_a) equal to 2.75% and a strain ratio (R_ε) equal to -1. In this figure, the cumulated plastic strain is plotted against the applied stress. The dash-dotted lines represent the simulations, while the dashed lines refer to the experiments. As can be seen, there is a very good agreement between the numerical results and the experimental data for the entire loading cycle. Overall, the elastic-plastic constitutive model captures well the cyclic stress-strain response of the tested alloy, either at the peak tensile stage or the peak compressive stage, which validates the proposed methodology.

4. Results and discussion

4.1 Cyclic stress-strain response

The cyclic stress-strain response of the tested alloy under constant-amplitude and step loading is summarised in Figure 4. Regarding the constant-amplitude tests, as can be seen, the material exhibited a mixed hardening-softening behaviour. At lower strain amplitudes, i.e. $\varepsilon_a \leq$ 1.00%, the cyclic response was characterised by strain-softening (see Fig. 4(a)). On the contrary, for strain amplitudes higher than 1.00%, it was observed a strain-hardening behaviour (see Fig. 4(b)). However, irrespective of the strain amplitude, the changes of the hysteresis loops during the tests were relatively small. This behaviour relatively independent from the load history can be explained by the face-centred cubic structure with high stacking fault energy which eases the cross slip during cyclic loading [22].

Concerning the two-step loading tests, as can be seen in Figure 4(c) and Figure 4(d), the cyclic stress-strain response of the higher steps is also quite stable, regardless of the loading sequence. Under lower strain amplitudes, the variations of the hysteresis loops are more expressive, which can be explained by the mean stress effect since these steps are not symmetrical. It is also clear that the peak compressive stresses tend to decrease with the increase of the loading cycles, either for the high-low sequence or the low-high sequence. Nevertheless, the peak tensile stresses behave differently, maintaining a constant value during the test for both loading sequences.

The transient behaviour associated with the cyclic response in strain control can be better analysed using dependent parameters. Figure 5(a) plots the stress amplitude against the number of cycles for different constant-amplitude and step loading tests. Regarding the constant-amplitude loading tests, we can see a mixed softening-hardening behaviour. At higher strain amplitude, i.e. ε_a = 1.25%, the softening response is characterised by a small reduction of stress amplitude during the first cycles followed by a slight increase until a saturated-like stage is reached. At lower strain amplitude, i.e. ε_a = 0.70%, hardening is observed throughout the entire lifetime. In the first few cycles, the hardening degree is higher. After this initial stage, the increase of stress amplitude is tenuous until the final failure.

Concerning the step loading tests, the stress responses are similar to those observed for constant-amplitude loading during most of the test. For the highest level of the high-low sequence, the stress amplitude is basically similar to that of the case conducted under constant-amplitude, which is expected since the loading scenarios are similar. However, when the second step starts, which is an asymmetrical one, the stress amplitude suddenly moves away from the values of the case conducted under constant-amplitude and then the material strain-hardens during a short initial period. After this period, the curves of the constant-amplitude and step loading tests tend to overlap.

As far as the low-high sequence is concerned, the response at the lowest level, which is characterised by an asymmetrical pattern, is slightly different from that of the case conducted at the same strain amplitude with R_{ε} = -1. The degree of strain-hardening of this first step is clearly smaller. In the second step, which is symmetrical, the values of stress amplitude sudden increase, denoting a strain-hardening response. After that, there is a progressive reduction until the final failure. It is also interesting to note that the values of stress amplitude are relatively close to those of the case tested under fully-reversed constant-amplitude loading. Moreover, the fatigue lives of both step loading tests are similar to each other and are between those obtained at constant amplitude for the higher and the lower strain amplitudes.

The hysteresis loop development during the test is another important aspect under strain-control mode. Based on the previous analysis, it can be hypothesised that the shape variations are not particularly expressive for this alloy. Figure 5(b) shows the variation of the plastic strain energy density per cycle (ΔW_p) with the number of cycles for constant-amplitude and step loading sequences. Overall, at the highest strain amplitudes, irrespective of the loading scenario, the values of plastic strain energy density per cycle are constant throughout the test. Nevertheless, at the lowest strain amplitudes, there is a small reduction of ΔW_p with the number of cycles, particularly at the first stage of the tests.

Under non-zero mean strain ($R_{\varepsilon} \neq$ -1), i.e. at the lowest strain levels of the step loading tests, mean stress relaxation phenomena were observed. The variation of mean stress with the number of cycles for different loading histories is exhibited in Figure 6(a). The degree of mean stress relaxation is higher at the beginning of the lowest strain level, either for high-low or low-high sequence, and then tends to a constant value. It is well-known that the mean stress relaxation gradients of a specific material are not only associated with the strain ratio, but also with the strain amplitude. In general, high-strength aluminium alloys relax more rapidly at higher strain amplitudes and at higher strain ratios [14-15]. The same trends were observed for the 7075-T651 aluminium alloy.

In relation to the highest strain levels of the two-step sequences, the mean stress values were close to zero during the entire lifetime, which is expected since such tests were conducted under fully-reversed conditions (see Figure 6(a)). In addition, these mean stress values were quite close to those found for constant-amplitude loading. In all cases, the stress values are slightly negative, which may be justified by the use of the nominal cross-section area in the calculation of both the maximum and minimum stresses. It is also interesting to note that the asymmetrical steps (R_ε = -0.12 and ε_a = 0.70%) do not fully relax, due to insufficient plastic strain in each cycle. This fact has been reported for other aluminium alloys [14,30].

The mean stress relation is likely to affect the position of the hysteresis loops with respect to the abscissa axis. The ratio of positive elastic strain energy density per cycle to the negative elastic strain energy density per cycle ($\Delta W_{e+}/\Delta W_{e-}$) can be used to investigate such variation. Figure 6(b) displays the variation of the $\Delta W_{e+}/\Delta W_{e-}$ ratio with the number of cycles for different loading histories, namely high-low sequence, low-high sequence, and constant-amplitude. Not surprisingly, under fully-reversed conditions, this ratio is close to unity, indicating a reasonable symmetry regarding the zero-stress coordinate line. On the other hand, it is also clear that the values of the $\Delta W_{e+}/\Delta W_{e-}$ ratio under fully-reversed conditions are similar, either for the constant-amplitude or the step loading tests.

In contrast, under non-zero mean strain, the above-mentioned ratio significantly deviates from unity, regardless of the loading sequence, as can be seen in Figure 6(b). There is a progressive change during the lifetime towards a stable value. Furthermore, the degree of relaxation is clearly dependent on the loading scenario, i.e. the lowest step of the high-low sequence ($\varepsilon_{a,1}$ = 1.25% and $\varepsilon_{a,2}$ = 0.70%) leads to more significant relaxation rates than that of the low-high sequence ($\varepsilon_{a,1}$ = 0.70% and $\varepsilon_{a,2}$ = 1.25%). Another important conclusion is that the $\Delta W_{e+}/\Delta W_{e-}$ ratio can better capture the asymmetries of the hysteresis loop shapes than the mean stress, which is an interesting outcome.

4.2 Stable response and fatigue lifetime

The stable stress-strain response of the tested alloy under fully-reversed conditions was examined from the mid-life hysteresis loops. Figure 7 compares the recorded shapes at different strain amplitudes with those simulated using the numerical model described in Section 3. For the sake of comparability, the compressive tips of the hysteresis loops are made to coincide. In general, as can be seen in the figure, experimental results and numerical simulations are in good agreement, particularly for the upper branches. Concerning the lower branches, we can identify more significant differences, but still close to the experimental cyclic response, which validates the proposed methodology.

It is also interesting to note that the upper branches of the hysteresis loops do not follow a unique curve. This demonstrates that the 7075-T651 aluminium alloy does not exhibit a Masing-type behaviour. Masing materials are those for which the upper branches of the hysteresis loops obtained at different strain amplitudes coincide when the lower tips are moved to a common origin which corresponds to the maximum compressive stress (see Figure 7). The violation of the Masing behaviour is attributed to an insufficient elastic region of the hysteresis loops, generally associated with the dislocation density and the cell size [31]. In the literature, there are several examples of aluminium alloys identified as non-Masing materials [14,31-33].

The strain-life curves obtained from the fully-reversed constant-amplitude fatigue tests are displayed in Figure 8(a). In the studied range, as can be seen in the figure, the plastic strain versus life and the elastic strain versus life relationships were successfully fitted by linear functions. It was also observed that the fitted functions correlated very well with the results available in the literature (see black markers) for this aluminium alloy [34]. On the other hand, it can also be concluded that the strain-life data points computed from the hysteresis loops simulated numerically are in good agreement with those determined in the experiments. The more relevant differences occurred for the lowest strain amplitudes.

Figure 8(b) plots both the plastic strain energy density per cycle (ΔW_p) versus life relationship and the total strain energy density per cycle (ΔW_t) versus life relationship determined from the experimental hysteresis loops collected from the constant-amplitude fatigue tests. A linear function was found to better represent the $\Delta \mathrm{W_p}$-life relationship. The tensile elastic energy at the material fatigue limit (ΔW_{0t}) of the $\Delta \mathrm{W_t}$-life relationship was estimated for 1×10^6 cycles. Regarding the energy-life data points obtained from the simulated hysteresis loops, no relevant differences were observed when compared to the experimental results.

The accurate simulation of the saturated hysteresis loops under fully-reversed conditions, as demonstrated above, opens interesting perspectives to the development of an robust fatigue life prediction model. However, it is still needed to investigate the hysteresis loop shapes obtained for the asymmetrical loading scenarios. A comparison for four different cases is presented in Figure 9. The dashed lines represent the loops simulated with the proposed approach, while the full lines correspond to the mid-life cycle of the lowest strain level (i.e. $R_\varepsilon \neq$ -1) of the high-low loading sequences.

As can be seen in the above-mentioned figure, the numerical and the experimental stress-strain responses are rather similar, particularly for the tensile tips, which are perfectly overlapped, irrespective of the strain amplitude or the strain ratio. With regard to the compressive tips, the conclusions are slightly different. The points are also overlapped for lower strain amplitudes, but they slightly deviate for higher strain amplitudes. Nevertheless, in any case, we can consider that the extreme points are close to each other. Thus, it makes possible the development of a robust fatigue life prediction model, provided that an adequate fatigue damage accumulation law is considered.

4.3 Fatigue life prediction

Fatigue life predictions were performed using three well-known models sensitive to mean stress in conjunction with a linear damage accumulation law. The models are based on the Coffin-Manson (CM), Smith-Watson-Topper (SWT), and Total Strain Energy Density (TSED) parameters. The damage accumulation law is based on the Palmgren-Miner damage rule. The three models as well as the linear damage accumulation rule are described below.

The Coffin-Manson (CM) model, with the mean stress correction of the elastic term introduced by Morrow, can be written as follows [35-36]:

$$\varepsilon_a = \frac{\left(\sigma_f' - \sigma_m\right)}{E}\,(2\mathrm{N_f})^b + \varepsilon_f'\,(2\mathrm{N_f})^c \tag{5}$$

where ε_a is the strain amplitude, σ_f' is the fatigue strength coefficient, b is fatigue strength exponent, ε_f' is the fatigue ductility coefficient, c is the fatigue ductility exponent, and σ_m is the mean stress.

The model based on the Smith-Watson-Topper (SWT) parameter is usually defined by the following formula [37]:

$$\varepsilon_a\,\sigma_{max} = \frac{\left(\sigma_f'\right)^2}{E}\,(2\mathrm{N_f})^{2b} + \sigma_f'\,\varepsilon_f'\,(2\mathrm{N_f})^{b+c} \tag{6}$$

where ε_a and σ_{max} are, respectively, the strain amplitude and the maximum stress, σ_f' is the fatigue strength coefficient, b is the fatigue strength exponent, ε_f' is the fatigue ductility coefficient, c is the fatigue strength exponent, and E is Young's modulus.

The total strain energy density (TSED) is another fatigue quantifier often used to account for mean stress effects [38]:

$$\Delta W_t = \kappa_t \, (2N_f)^{\alpha_t} + \Delta W_{0t} \quad (7)$$

where κ_t and α_t are material constants, and ΔW_{0t} is the tensile elastic energy at the material fatigue limit. Here, it is defined by the sum of both the elastic positive strain energy density per cycle, and the plastic strain energy density per cycle (see Figure 6(b)).

The cumulative fatigue damage was calculated using the Palmgren-Miner damage rule. For two-step loading conditions, it leads to [18-20]:

$$\frac{n_1}{N_1} + \frac{n_2}{N_2} = 1 \quad (8)$$

where n_1 and n_2 are the number of cycles applied at the first and the second strain levels, respectively; and N_1 and N_2 are the fatigue life at the first and the second strain level.

Predicted fatigue lives versus observed fatigue lives for the studied loading histories, computed from the three fatigue models in conjunction with the cumulative damage rule, are presented in Figure 10. In this first analysis, the fatigue variables (i.e. strain amplitude, mean stress, maximum stress, SWT-damage parameter, and total strain energy density) were computed from the mid-life hysteresis loops obtained experimentally. As can be seen in the figure, the CM-based and the SWT-based results show a close correlation between the fatigue life and the loading history, either for the high-low sequence or the low-high sequence. On the contrary, the TSED-based approach is less accurate, leading to unsatisfactory results in some cases.

It is worth to note that the predictions based on the SWT parameter fall within a narrow range, and are tendentially conservative, which is another interesting finding. In the case of the CM-based model, although the data points are also well correlated, they are spread in a wider range, and are either conservative or non-conservative. These results clearly demonstrate that both the CM-based and the SWT-based approaches, in conjunction with the Palmgren-Miner linear damage rule, can appropriately capture the effect of load sequence on fatigue behaviour for the tested aluminium alloy under two-step loading.

Since the simulated hysteresis loops are close to the experimental ones, it is reasonable to admit that the fatigue life predictions based on the numerical simulations of the cyclic stress-strain response are likely to be sufficiently robust. The predicted fatigue lives and the observed fatigue lives computed from the simulated hysteresis loops, using the CM-based and the SWT-based models, are compared in Figure 11. In this approach, the fatigue variables (i.e. strain amplitude, mean stress, and maximum stress) were determined from the numerically simulated loops. For the sake of comparability, the data points corresponding to the experimental-based approach (i.e. those plotted in Figure 10) are represented in grey.

As can be seen in the above-mentioned figure, the quality of results computed by means of the proposed strategy is relatively similar to those obtained from the experimental hysteresis loops, either for the CM-based model, or the SWT-based model. In general, we can see that the data points are slightly less conservative. However, there is a good correlation between the calculated fatigue lives and the observed fatigue lives for both models, irrespective of the loading sequence. Particularly for the SWT-based model, the results are within scatter bands of factors of 1.5 and most of them evidence a very low scatter. This demonstrates that the numerical-based approach is sensitive to the load sequence effect.

In order to better evaluate the predictive capabilities of the tested approaches, a statistical study based on the probability density functions of the prediction error was carried out. Here the prediction error (P_E) was defined by the following formula:

$$P_E = \text{Log}\ (N_e) - \text{Log}\ (N_p) \qquad (9)$$

where N_e is the experimentally observed fatigue life, and N_p is the predicted fatigue life. More accurate models are generally associated with lower standard deviations and mean errors close to zero. As hypothesised above, the SWT-based models better capture the load sequence effects on fatigue behaviour than the CM-based models because the mean errors are closer to zero and the standard deviations are smaller. Moreover, it can be observed that the numerical approaches are more shifted to the non-conservative side than the experimental ones. Apart from that, the probability density functions are relatively similar.

To conclude this section, we would like to emphasise that the proposed numerical tool is capable of capturing the effect of loading history on the fatigue behaviour of the 7075-T651 aluminium alloy under two-step loading sequences. It only requires a simple strain-life curve and an elastic-plastic constitutive model, which can be met by a series of standard fully-reversed strain-controlled tests. Therefore, the predictive approach is simplified, since a limited number of fatigue tests is necessary, and ultimately the cost and time associated with the calculations are significantly reduced. Last but not least, the proposed numerical tool is suitable for industrial application.

5. Conclusions

The paper studied the load sequence effect on cyclic deformation and fatigue behaviour of 7075-T651 aluminium alloy under two-step loading. High-low and low-high sequences, encompassing both symmetrical and asymmetrical steps, were performed under strain-controlled mode for different loading scenarios. The stabilised stress-strain response was simulated numerically using an elastic-plastic constitutive model. Fatigue life was predicted by combining a linear damage accumulation rule with the CM-based, SWT-based, and TSED-based parameters. The following conclusions can be drawn:

- A constitutive model based on the von Mises yield criterion coupled with a mixed isotropic-kinematic hardening has been adequate to simulate the stabilised stress-strain response of the tested alloy under strain-control mode for symmetrical and asymmetrical loading cases;
- Under fully-reversed strain-controlled materials, the material exhibited a mix cyclic hardening-softening behaviour. It hardened for strain amplitudes higher than 1.0% and exhibited a softening response below this value. However, the changes of the hysteresis loops were relatively small;
- In the two-step loading cases, a hardening behaviour was observed during a short initial period, when the second step was applied. After this period, the responses under

constant- and two-step loading were similar. The degree of strain-hardening was affected by the load sequence;

- Mean stress relaxation was also affected by the load sequence. Higher mean stress relaxation rates were observed in the beginning of the asymmetrical steps. Moreover, high-low sequences led to higher mean stress relaxation rates than the low-high sequences;
- The linear damage accumulation rule in conjunction with the SWT damage parameter provided better fatigue life predictions than the models based on the strain-life and energy-life relationships. This was attributed to the fact that this fatigue quantifier includes stress and strain terms, making it more sensitive to load sequence effects.
- Fatigue life predictions computed from the hysteresis loops simulated numerically using the CM-based and the SWT-based models were close to those obtained from the experimental hysteresis loops. The latter led to better life predictions with all points within scatter bands of factors of 1.5.

Acknowledgements

This research is sponsored by FEDER funds through the program COMPETE – Programa Operacional Factores de Competitividade – and by national funds through FCT – Fundação para a Ciência e a Tecnologia – under the project UIDB/00285/2020.

References

1. Ashkenazi D (2019). How aluminum changed the world: a metallurgical revolution through technological and cultural perspectives. Technological Forecasting and Social Change 143, 101–13.
2. Zhang X, Chen Y, Hu J (2018). Recent advances in the development of aerospace materials. Progress in Aerospace Sciences 97, 22–34.
3. Carpinteri A, Vantadori S, Łagoda T, Karolczuk A, Kurek M, Ronchei C (2018). Fatigue assessment of metallic components under uniaxial and multiaxial variable amplitude loading. Fatigue and Fracture of Engineering Materials and Structures 41, 1306-1317.
4. Zhu SP, Liao D, Liu Q, Correia JAO, Jesus AMP (2020). Nonlinear fatigue damage accumulation: Isodamage curve-based model and life prediction aspects. International Journal of Fatigue Volume 128, 105185
5. Vantadori S, Carpinteri A, Fortese G, Ronchei C, Scorza D, Zanichelli A (2018). Fatigue lifetime evaluation of notched components: Implementation of the control volume

concept in a strain-based LCF criterion. Theoretical and Applied Fracture Mechanics 97, 400-408.

6. Liao D, Zhu SP, Correia JAFO, De Jesus AMP, Berto F (2020). Recent advances on notch effects in metal fatigue: A review. Fatigue and Fracture of Engineering Materials and Structures 43, 637-659.
7. Negru R, Șerban DA, Marșavina L, Magda A (2016). Lifetime prediction in medium-cycle fatigue regime of notched specimens. Theoretical and Applied Fracture Mechanics 84, 140-148.
8. Zakaria KA, Abdullah S, Ghazali MJ (2016). A review of the loading sequence effects on the fatigue life behaviour of metallic materials. Journal of Engineering Science and Technology Review 9, 189-200.
9. Marciniak Z, Rozumek D, Macha E (2008). Fatigue lives of 18G2A and 10HNAP steels under variable amplitude and random non-proportional bending with torsion loading. International Journal of Fatigue 30, 800-813.
10. Necemer B, Zupanic F, Gabriel D, Tarquino E, Sraml M, Glodez S (2021). Low cycle fatigue behaviour of ductile aluminium alloys using the inelastic energy approach. Materials Science and Engineering A 800, 140385."
11. Long XY, Branco R, Zhang FC, Berto F, Martins RF (2020). Influence of Mn addition on cyclic deformation behaviour of bainitic rail steels. International Journal of Fatigue 132, 105362.
12. Koh SK, Oh SJ, Li C, Ellyin F (1999). Low-cycle fatigue life of SiC-particulate-reinforced Al-Si cast alloy composites with tensile mean strain effects. International Journal of Fatigue 21, 1019–1032.
13. Linul E, Serban DA, Marsavina L, Kovacik J (2016). Low-cycle fatigue behaviour of ductile closed-cell aluminium alloy foams. Fatigue and Fracture of Engineering Materials and Structures 40, 597-604.
14. Branco R, Costa JD, Borrego LP, Wu SC, Long XY, Zhang FC (2019). Effect of strain ratio on cyclic deformation behaviour of 7050-T6 aluminium alloy. International Journal of Fatigue 129, 105234.
15. Sandor BI. Fundamentals of cyclic stress and strain. University of Wisconsin Press; 1972, ISBN: 978-0299061005.
16. Hectors K, Waele W (2021). Cumulative damage and life prediction models for high-cycle fatigue of metals: a review. Metals 11, 204.
17. Fatemi A, Yang L (1998). Cumulative fatigue damage and life prediction theories: a survey of the state of the art for homogeneous materials. International Journal of Fatigue 20, 9-34

18. Miner MA (1954). Cumulative damage in fatigue. Journal of Applied Mechanics 67, AI59-AI64.
19. Zhu SP, Hao Y-Z, Correia JAFO, Lesiuk G, Jesus AMP (2019). Nonlinear fatigue damage accumulation and life predictionof metals: A comparative study. Fatigue and Fracture of Engineering Materials and Structures 42, 1271-1282.
20. Lv Z, Huang H-Z, Zhu S-P, Gao H, Zuo F (2015). A modified nonlinear fatigue damage accumulation model. International Journal of Damage Mechanics 24(2), 168–181.
21. Topper TH, Sandor BI, Morrow J (1969). Cumulative fatigue damage under cyclic strain control. Journal of Materials 4, 189–199.
22. Colin J, Fatemi A (2010). Variable amplitude cyclic deformation and fatigue behaviour of stainless steel 304L including step, periodic, and random loadings. Fatigue and Fracture of Engineering Materials and Structures 33, 205-220.
23. Zhao X, Li H, Chen T, Cao B, Li X (2019). Mechanical properties of aluminum alloys under low-cycle fatigue loading. Materials 12, 2064.
24. Cunha J, Mateus A, Malça C, Costa J, Branco R (2021). Effect of strain load history on fatigue behaviour of the 7075-T651 aluminium alloy. Sustainability and Automation in Smart Constructions. Advances in Science, Technology & Innovation, pages 279-284, Springer.
25. S.P. Zhu, Q. Lei, Q.Y. Wang (2017) Mean stress and ratcheting corrections in fatigue life prediction of metals. Fatigue and Fracture of Engineering Materials and Structures 40(9), 1343-1354.
26. Agius D, Kourousis K, Wallbrink C (2018). A modification of the multicomponent Armstrong–Frederick model with multiplier for the enhanced simulation of aerospace aluminium elastoplasticity. International Journal of Mechanical Sciences 144, 118–133.
27. Nath A, Barai S, Ray K (2019). Prediction of asymmetric cyclic-plastic behaviour for cyclically stable non-ferrous materials. Fatigue and Fracture of Engineering Materials and Structures 42, 2808–2822.
28. Lasdon LS, Waren AD, Jain A, Ratner MW. Design and testing of a generalized reduced gradient code for nonlinear optimization. NTIS National Technical Information Service U. S. Department of Commerce, Cleveland. 1975.
29. Oliveira MC, Alves JL, Menezes LF (2008). Algorithms and strategies for treatment of large deformation frictional contact in the numerical simulation of deep drawing process. Archives of Computational Methods in Engineering 15, 113–162.

30. Hao H, Ye D, Chen C (2014). Strain ratio effects on low-cycle fatigue behavior and deformation microstructure of 2124–T851 aluminum alloy. Materials Science and Engineering A 605, 151–159.
31. Plumtree A, Abdel-Raouf HA (2001). Cyclic stress–strain response and substructure. International Journal of Fatigue 23, 799–805.
32. Rusk DT, Taylor RE, Hoffman PC (2006). Testing of 7050-T7451 aluminium strain-life coupons for a probabilistic strain-life curve. Department of the Navy Naval Air Warfare Center Aircraft Division, Maryland, Report NAWCADPAX/TR-2006/140.
33. Branco R, Costa JD, Borrego LP, Wu SC, Long XY, Antunes FV (2020). Effect of tensile pre-strain on low-cycle fatigue behaviour of 7050-T6 aluminium alloy. Engineering Failure Analysis 114, 104592.
34. Zhao T, Jiang Y (2008). Fatigue of 7075-T651 aluminum alloy. International Journal of Fatigue 30, 834–849.
35. Manson SS (1954). Beahaviour of materials under conditions of thermal stress. NACA TN-2933, National Advisory Committee for Aeronautics.
36. Morrow JD (1965). Cyclic plastic strain energy and fatigue of metals. International Friction, Damping and Cyclic Plasticity, American Society for Testing and Materials, ASTM STP 378, Philadelphia, 45-87.
37. Smith R, Watson TH, Topper T (1970). A stress-strain parameter for the fatigue of metals. Journal of materials JMLSA 5, 767–778.
38. Golos K, Ellyin F (1988). A total strain energy density theory for cumulative damage. Journal of Pressure Vessel Technology 110, 36–41.

Tables

Table 1. Nominal chemical composition of the 7075-T651 aluminium alloy (wt.%)

Zn	Mg	Cu	Si	Fe	Mn	Al
4.89	2.12	1.52	0.33	0.007	0.09	Balance

Table 2. Mechanical properties of the tested 7075-T651 aluminium alloy

Young's modulus, E (GPa)	71.7
Yield strength, σ_{YS} (MPa)	503
Ultimate tensile strength, σ_{UTS} (MPa)	561
Poisson's ratio, ν	0.306
Elongation at break (%)	11

Table 3. Summary of constant-amplitude (CA) and high-low (HL) and low-high (LH) tests

Sequence	$\varepsilon_{a,1}$ (%)	$R_{\varepsilon,1}$	$\varepsilon_{a,2}$ (%)	$R_{\varepsilon,2}$	n_1 (cycle)	n_2 (cycle)	N_f (cycle)
CA	0.50	-1	-	-	11084	-	11084
CA	0.70	-1	-	-	1325	-	1325
CA	0.80	-1	-	-	609	-	609
CA	1.00	-1	-	-	302	-	302
CA	1.25	-1	-	-	167	-	167
CA	1.50	-1	-	-	119		119
CA	1.75	-1	-	-	115	-	230
CA	2.25	-1	-	-	56	-	56
CA	2.75	-1	-	-	34	-	34
HL	1.50	-1	0.70	0.07	24	861	885
HL	1.25	-1	0.70	-0.12	33	559	592
HL	1.00	-1	0.70	-0.40	68	637	705
HL	1.50	-1	0.50	0.33	24	2893	2917
HL	1.25	-1	0.50	0.20	33	2091	2124
HL	1.00	-1	0.50	0	68	3719	3787
LH	0.70	0.07	1.50	-1	265	117	382
LH	0.70	-0.12	1.25	-1	265	150	415
LH	0.70	-0.40	1.00	-1	265	267	532
LH	0.50	0.33	1.50	-1	2216	48	2264
LH	0.50	0.20	1.25	-1	2216	26	2242
LH	0.50	0	1.00	-1	2216	319	2535

Figures

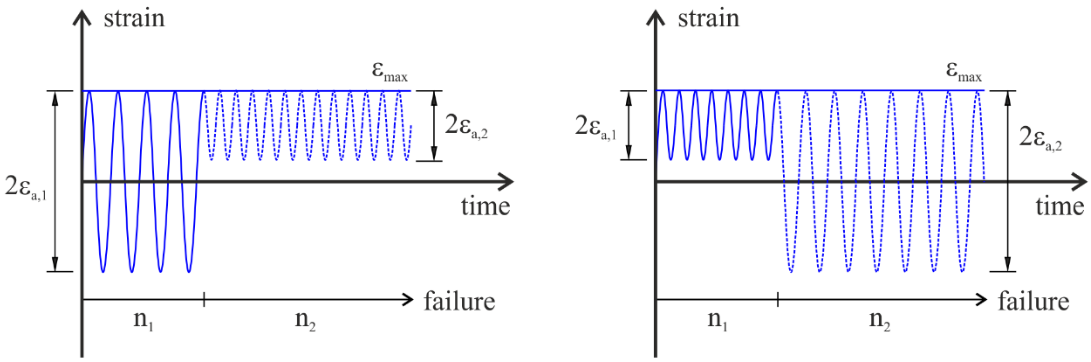

Figure 1. Cyclic loading histories: (a) high-low sequence; and (b) low-high sequence ($2\varepsilon_{a,1}$ and $2\varepsilon_{a,2}$ represent the strain ranges of step 1 and step 2, respectively; n_1 and n_2 represent the number of cycles applied in step 1 and step 2, respectively.

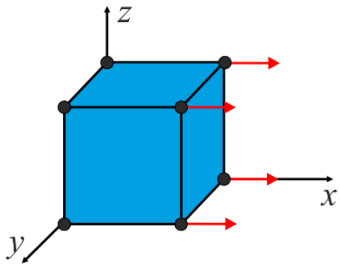

Figure 2. Finite element model used to simulate the saturated cyclic stress-strain response of the 7075-T651 aluminium alloy under strain-controlled conditions.

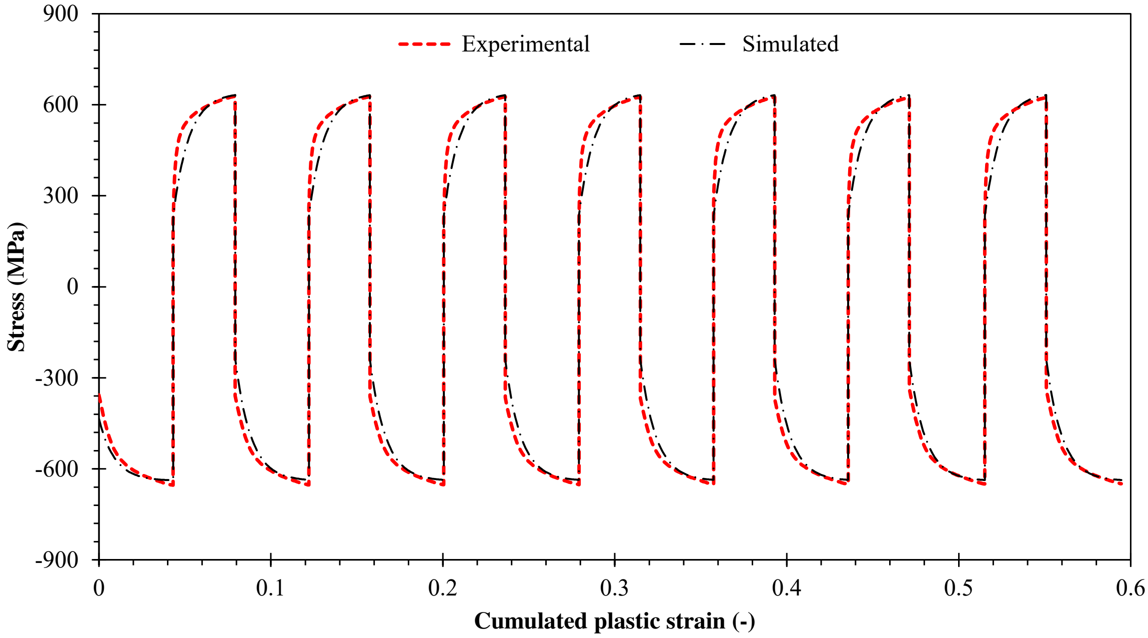

Figure 3. Numerical and experimental cyclic stress-strain responses of the 7075-T651 aluminium alloy under strain-controlled conditions at ε_a = 2.75% and R_ε = -1.

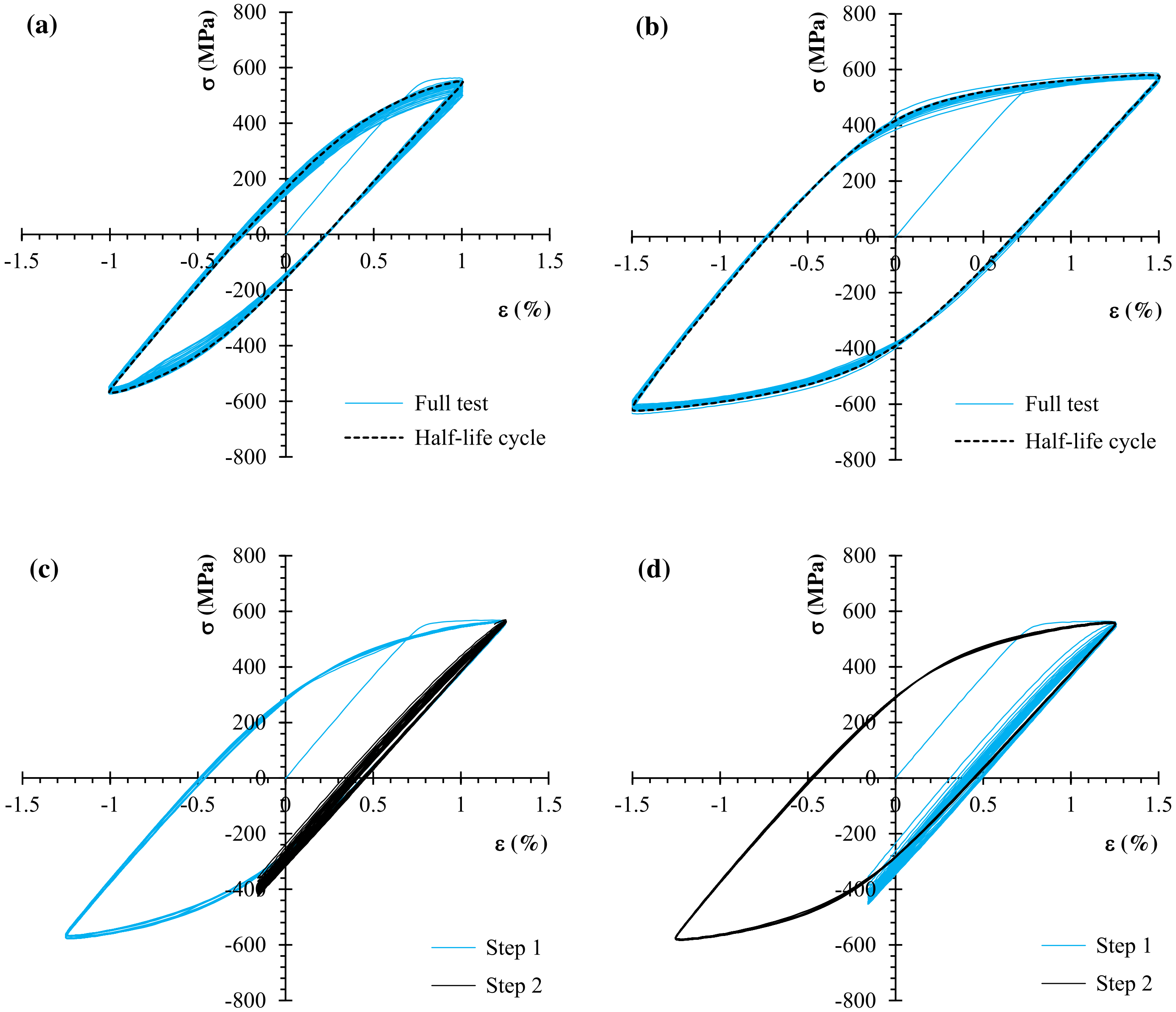

Figure 4. Cyclic hysteretic response of the 7075-T651 aluminium alloy under strain-controlled conditions: (a) constant-amplitude loading with ε_a = 1.00%; (b) constant-amplitude loading with ε_a = 1.25%; (c) high-low step loading with $\varepsilon_{a,1}$ = 1.25% and $\varepsilon_{a,2}$ = 0.70%; and (d) low-high step loading with $\varepsilon_{a,1}$ = 0.70% and $\varepsilon_{a,2}$ = 1.25%.

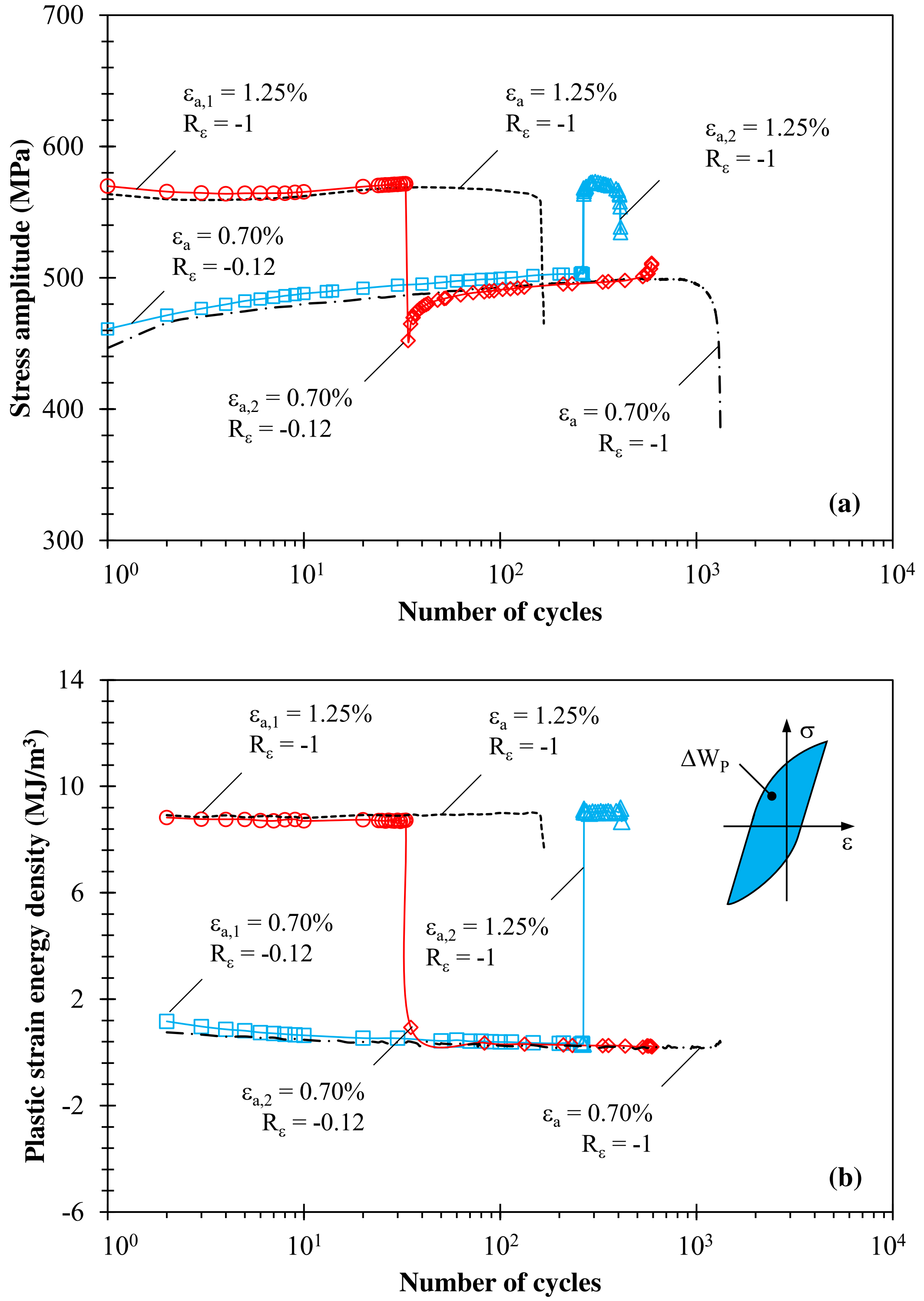

Figure 5. (a) Stress amplitude versus number of cycles; and (b) plastic strain energy density versus number of cycles.

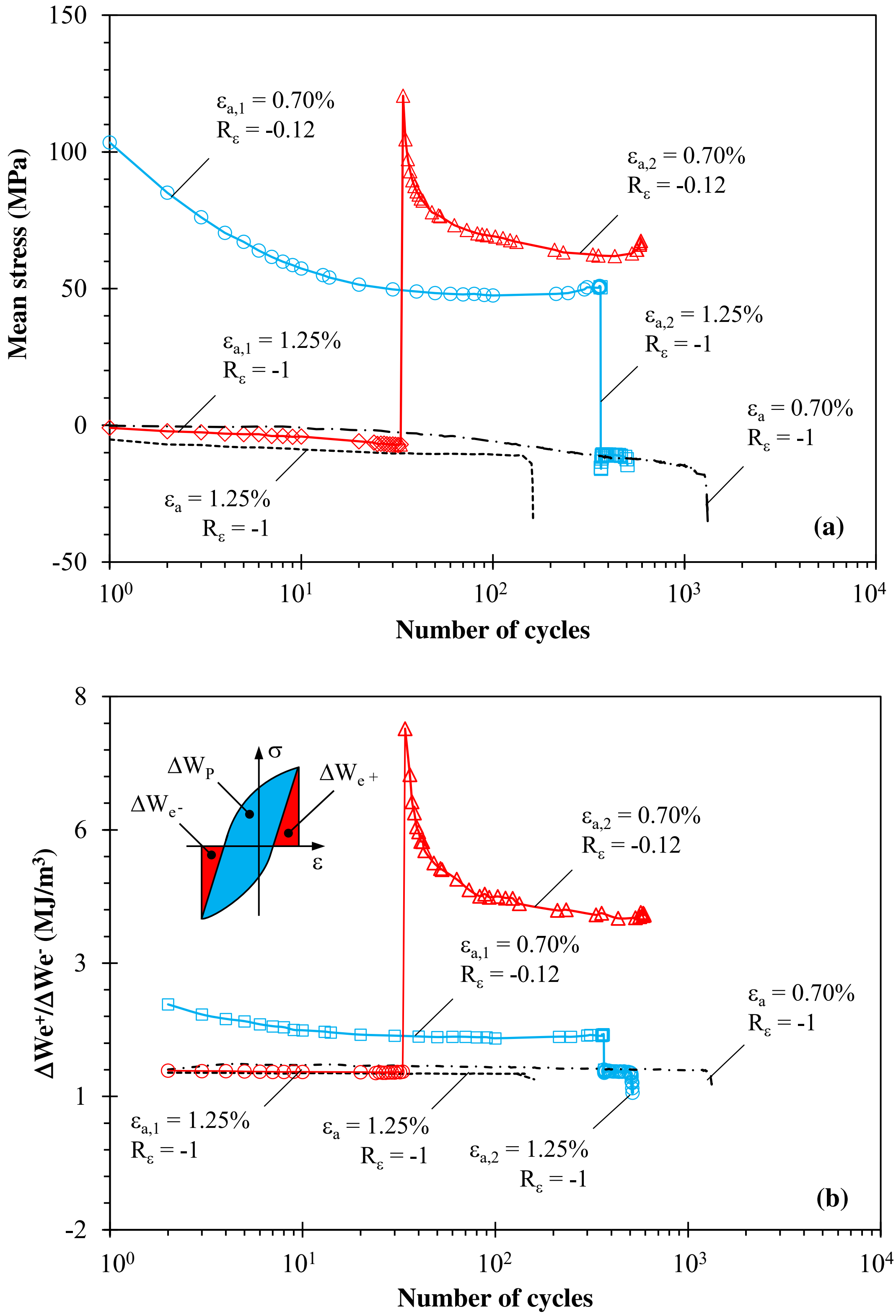

Figure 6. (a) Mean stress versus number of cycles; and (b) $\Delta W_{e+}/\Delta W_{e-}$ ratio versus number of cycles.

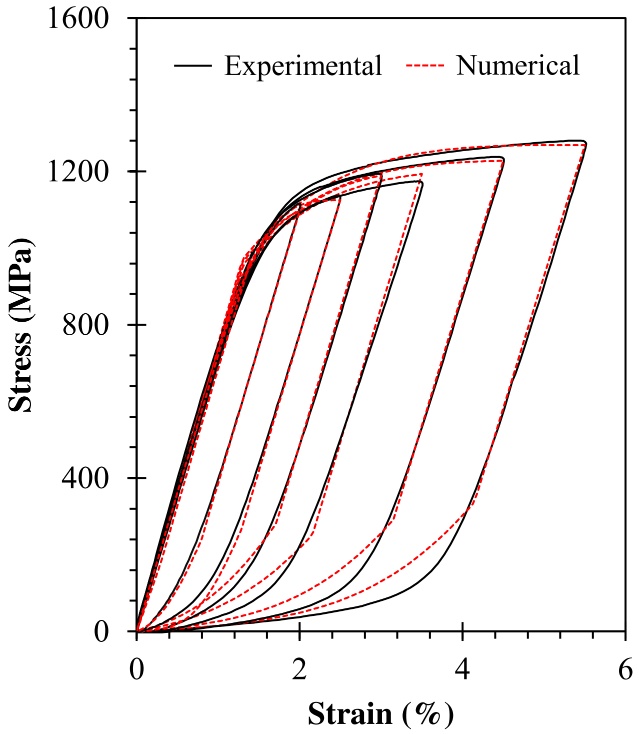

Figure 7. Comparison of experimental and numerical stable hysteresis loops, in relative coordinates, obtained under constant-amplitude loading tests. Experimental testes refer to the mid-life cycle.

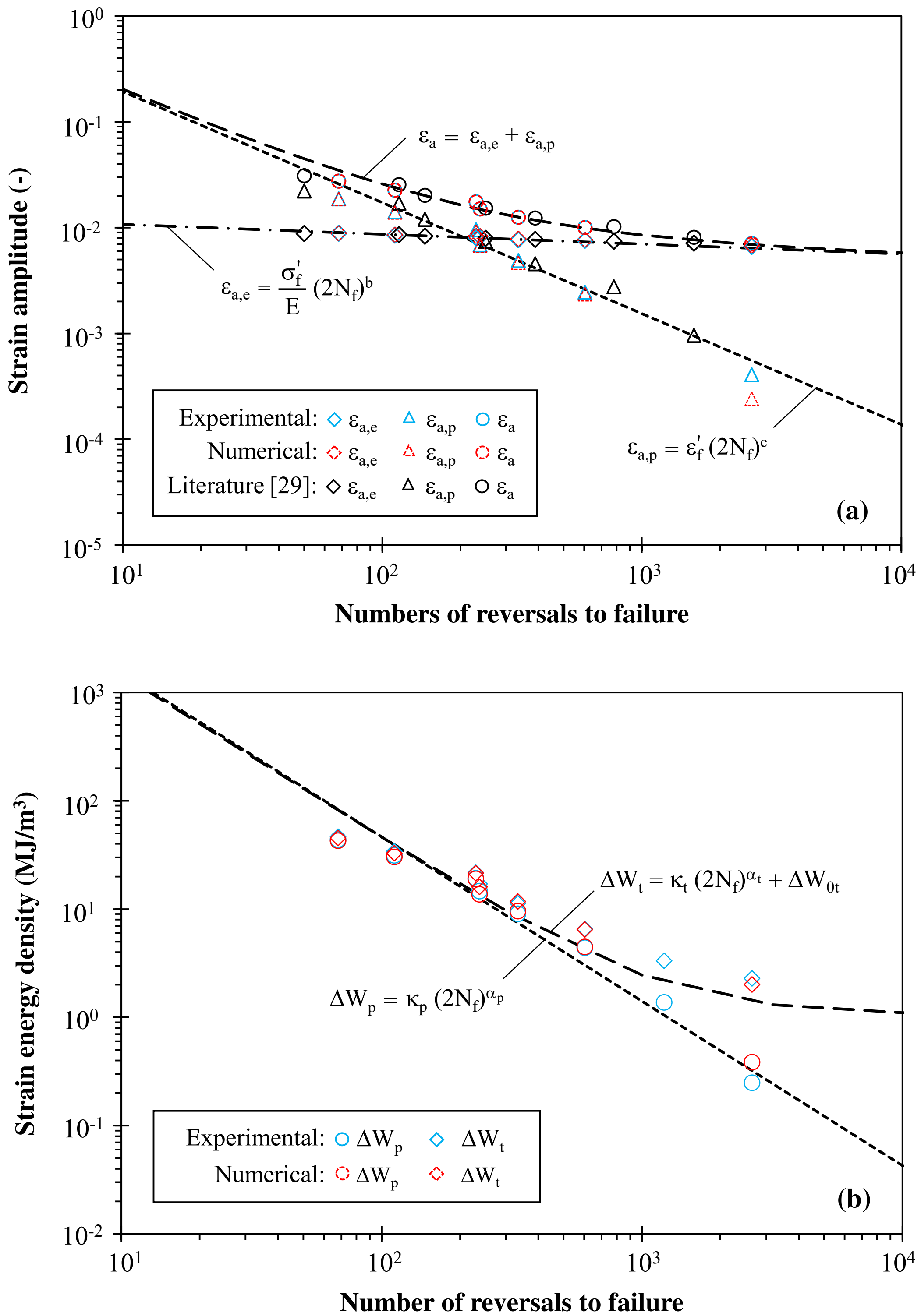

Figure 8. Strain-life curve (a) and energy-life curve (b) of the tested aluminium alloy under fully-reversed strain controlled conditions. Dashed lines represent the fitted functions determined from the experimental data.

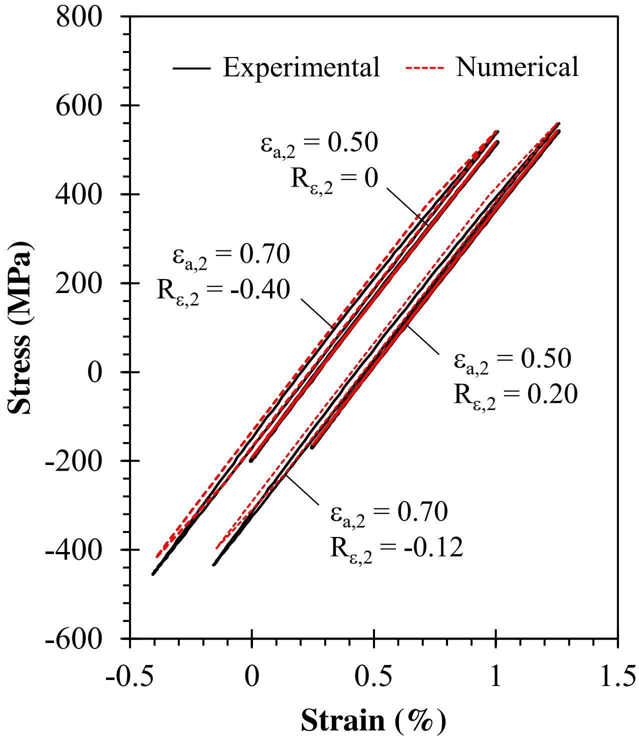

Figure 9. Comparison of experimental and numerical hysteresis loops obtained in the high-low tests for the asymmetrical steps. Experimental tests refer to the mid-life cycle.

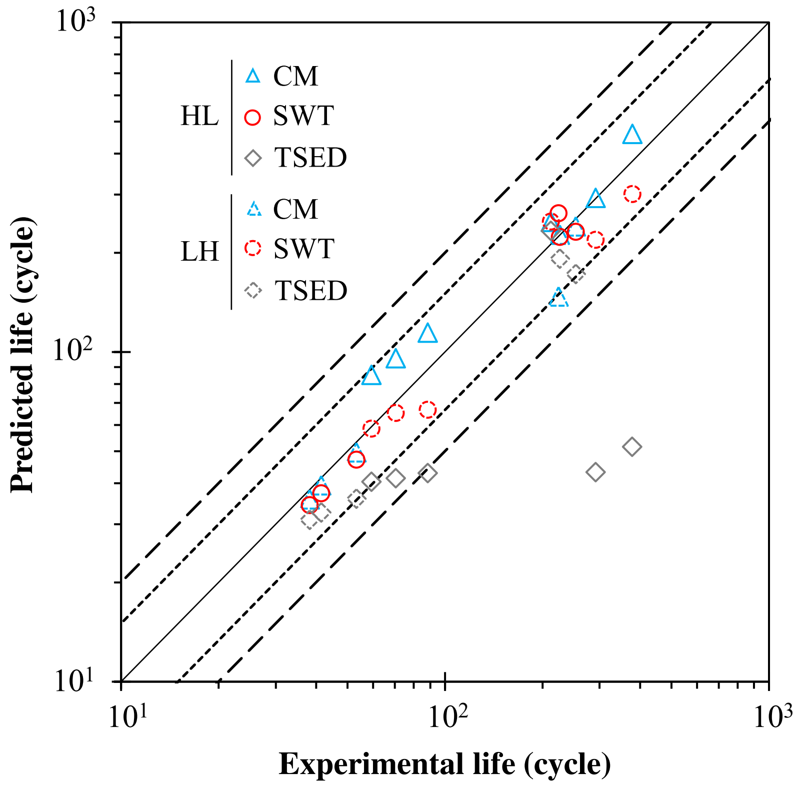

Figure 10. Comparison of the predicted fatigue lives and the observed fatigue lives for the loading sequence tests. Calculations were computed from the mid-life hysteresis loops obtained experimentally. Thinner and thicker dashed lines represent scatter bands of factors of 1.5 and 2.0, respectively.

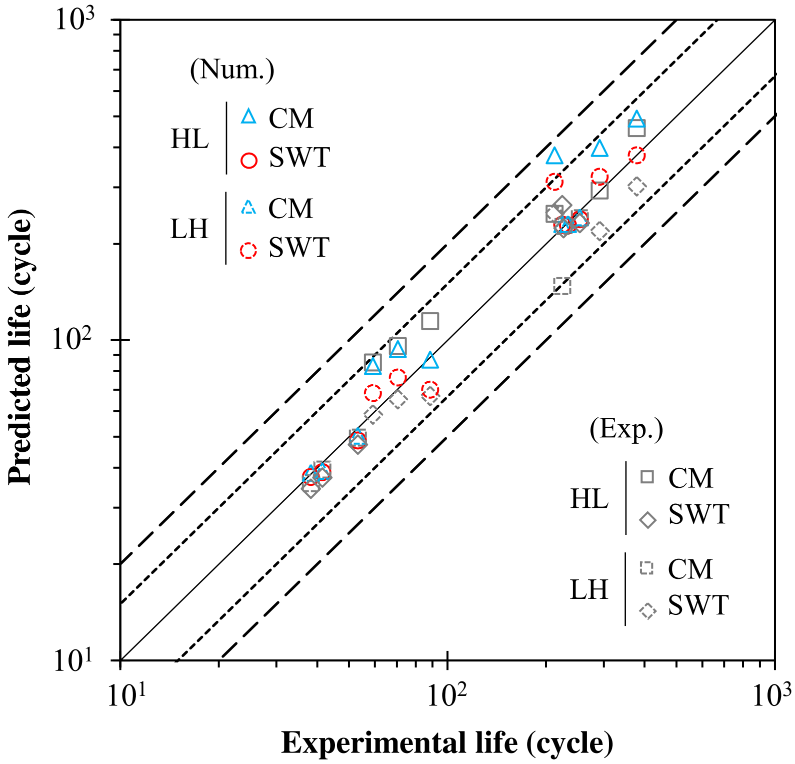

Figure 11. Comparison of the predicted fatigue lives and the observed fatigue lives for the loading sequence tests. Calculations were computed from the hysteresis loops simulated numerically. Thinner and thicker dashed lines represent scatter bands of factors of 1.5 and 2.0, respectively.

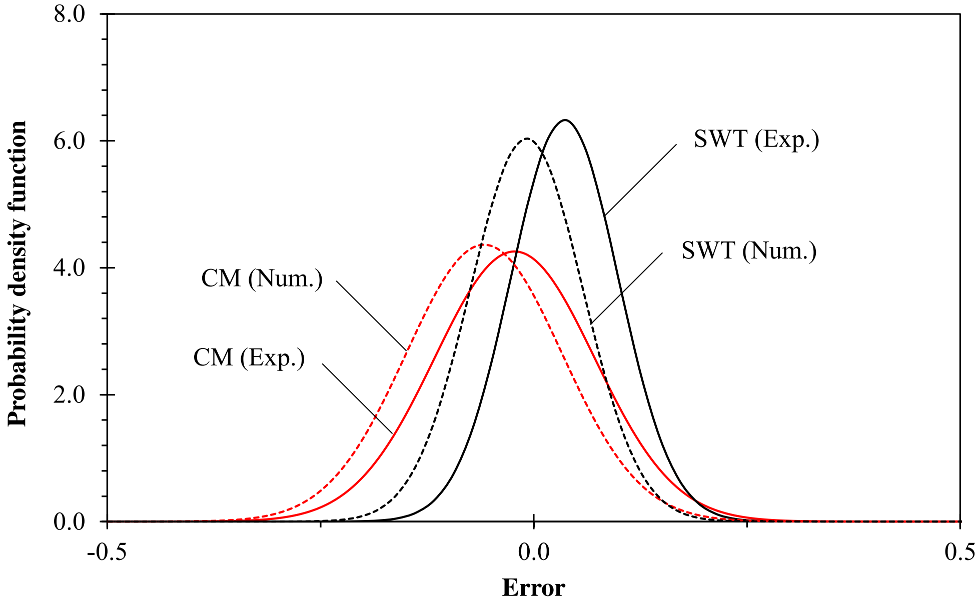

Figure 12. Probability density functions of the predictive error for the CM-based and SWT-based models. Full lines refer to the calculations carried out using the hysteresis loops collected in the experiments while the dashed lines refer to the calculations carried out using the hysteresis loops simulated numerically.

Declaration of interests

☒ The authors declare that they have no known competing financial interests or personal relationships that could have appeared to influence the work reported in this paper.

☐The authors declare the following financial interests/personal relationships which may be considered as potential competing interests:

Load sequence effects and cyclic deformation behaviour of 7075-T651 aluminium alloy

R. Branco[a], J.D. Costa[a], P.A. Prates[b,a], F. Berto[c], C. Pereira[d], A. Mateus[d]

[a] University of Coimbra, CEMMPRE, Department of Mechanical Engineering, Coimbra, Portugal

[b] Department of Mechanical Engineering, Centre for Mechanical Technology & Automation (TEMA), University of Aveiro, 3810-193 Aveiro, Portugal

[c] Department of Mechanical and Industrial Engineering, NTNU, 7491 Trondheim, Norway

[d] Centre for Rapid and Sustainable Product Development, Polytechnic Institute of Leiria, Rua de Portugal, Marinha Grande, 2430-028, Portugal

Load sequence effects and cyclic deformation behaviour of 7075-T651 aluminium alloy

R. Branco[a,1], J.D. Costa[a], P.A. Prates[b,a], F. Berto[c], C. Pereira[d], A. Mateus[d]

[a] University of Coimbra, CEMMPRE, Department of Mechanical Engineering, Coimbra, Portugal

[b] Department of Mechanical Engineering, Centre for Mechanical Technology & Automation (TEMA), University of Aveiro, 3810-193 Aveiro, Portugal

[c] Department of Mechanical and Industrial Engineering, NTNU, 7491 Trondheim, Norway

[d] Centre for Rapid and Sustainable Product Development, Polytechnic Institute of Leiria, Rua de Portugal, Marinha Grande, 2430-028, Portugal

Abstract

This paper investigates the effect of loading history on cyclic deformation and fatigue behaviour of 7075-T651 aluminium alloy subjected to two-step ~~variable-amplitude~~ loading. High-low and low-high sequences, encompassing both symmetrical and asymmetrical steps, are performed under strain-controlled mode for different loading scenarios. An elastic-plastic constitutive model is developed using the finite element method to simulate the stabilised stress-strain response. Fatigue life predictions are ~~performed~~ made by applying~~using~~ strain-based, energy-based, and SWT-based methods. The SWT-based model properly captured the effect of load history on fatigue behaviour. In addition, fatigue life predictions carried out using the numerical simulations agreed well with the experiments.

Keywords: load sequence; variable-amplitude loading; step loading; cumulative damage; linear damage rule; cyclic deformation; 7075-T651 aluminium alloy.

1. Introduction

Aluminium alloys have a major application in aviation, aerospace, and automotive industries due to their low density, high strength, good fracture toughness, and attractive cost [1-2]. In these areas of application, most components are exposed to variable-amplitude loading which makes them prone to fatigue failure [3-4]. On the other hand, although fatigue design often assumes that materials are loaded in the elastic range, at the critical geometric discontinuities, local plastic deformation can occur [5-7~~6~~]. Therefore, the development of robust engineer3~~i~~ng

[1] Corresponding author: R. Branco (ricardo.branco@dem.uc.pt)

design methods against fatigue requires not only the knowledge of the loading history but also an adequate understating of the cyclic deformation behaviour.

Material response to cyclic deformation (e.g. cyclic hardening, cyclic softening, mean stress relaxation, ratcheting) is not a trivial problem, because it is history dependent, i.e. the cyclic stress-strain response may significantly change with the load sequence [8-9]. It is also well-known that cyclic deformation response is material dependent [10-12]. Particularly in the case of aluminium alloys, because of they have face-centred cubic crystal structures with high stacking fault energy, their cyclic deformation response is less dependent on the loading history than that of other engineering materials, namely face-centred cubic metals with low stacking fault energy, which can be advantageous regarding the development of reliable fatigue design methods.

Another important aspect, not negligible, in fatigue design is the mean stress effect. Several attempts have been made in the past to account for such a phenomenon. Regarding precipitation-hardening aluminium alloys, literature shows that positive mean stresses are detrimental to fatigue life, while negative mean stresses are beneficial, and that mean stress relaxation rates depend on strain ratio, strain amplitude, and material type [~~1~~13-14~~2~~]. In addition, under strain-controlled conditions, when there is full relaxation of mean stress, fatigue life is not significantly affected. It is also known that cyclic softening materials, such as high-strength aluminium alloys, are more susceptible to mean stress relaxation than cyclic hardening materials [15~~3~~].

In a design point of view, fatigue life assessment under variable-amplitude loading requires an accurate calculation of damage accumulation. Cumulative fatigue damage theories have attracted much attention overt the last decades [16~~4~~-17~~5~~]. Although there are many approaches available in the literature, the most commonly used, partly due to its simplicity, is the so-called Palmgren-Miner rule, which assumes that damage is accumulated linearly [18~~6~~]. Its most obvious shortcoming is the inability to deal with load sequence effects. Due to the triangular relationship between load sequence, damage accumulation, and fatigue life, such effects cannot be ignored. A comprehensive discussion about the most relevant theories to deal with load interaction effects can be found in the papers by Zhu et al. [19,20].

So far, very few studies have addressed the effect of loading sequence on fatigue life in aluminium alloys subjected to uniaxial strain-controlled conditions [21~~17~~-24~~0~~]. Colin an Fatemi

[18] concluded that a fatigue model based on the Smith-Watson-Topper (SWT) parameter in conjunction with a linear damage rule can capture the load sequence effect. When compared to the commonly used methods that combine the above-mentioned damage rule with conventional stress-life or strain-life relationships, the fatigue life predictions were considerably better. This improvement was attributed to the fact that the SWT parameter includes both stress and strain terms, making it more suitable for deformation-sensitive materials. Additionally, it is able to account for mean stress effects [25].

Experimental analysis of load sequence effects on cyclic deformation behaviour and fatigue life, particularly for realistic geometries and in-service loading spectra, is expensive and time-consuming. With the advent of computer technology, numerical methods can be advantageously introduced to develop precise cyclic constitutive models, allowing the simulation of different load histories quickly and cheaply [26~~1~~-27~~2~~]. Regarding the 7075-aluminium alloy, limited work has been published on cyclic constitutive models. Two exceptions are the recent papers by Agius et al. [26~~1~~] and Nath et al. [27~~2~~]. However, the focus has been put on hysteresis loop development; the effect of loading history on the fatigue life has not been addressed.

The present paper aims to study the load sequence effect on both the cyclic plastic behaviour and the fatigue life in the 7075-T651 aluminium alloy under two-step~~variable-amplitude~~ loading. Firstly, experimental ~~two-step load~~ tests encompassing both high-low and low-high sequences are performed for the studied material under strain-controlled mode. Then, an elastic-plastic model is developed from fully-reversed constant-amplitude data to simulate the stabilised stress-strain response. Finally, fatigue life predictions are performed using strain-based, energy-based, and SWT-based methods and the damage accumulation is accounted for with ~~the~~ a linear damage rule.

2. Material and methods

The material studied in this research was the 7075-T651 aluminium alloy supplied in the form of a 35mm-thick plate. Its nominal chemical composition and its main monotonic tensile properties are listed in Table 1 and Table 2, respectively. Two types of cylindrical specimens, machined according to ASTM E606 standard, were tested: one with a 19mm-long and 6mm-diameter gauge section, and another with a 15mm-long and 8mm-diameter gauge section. In order to prevent buckling problems, the former was used for lower strain amplitudes, while the latter was used for higher strain amplitudes.

The tests were carried out at room temperature under uniaxial strain-control mode using sinusoidal waves and a constant strain rate (8×10^{-3} s^{-1}). Failure was defined as 40% load drop from the first cycle, or fracture, whichever occurred first. The cyclic stress-strain response was recorded using a 12.5mm-long mechanical extensometer clamped directly to the gauge section of the specimen. Silicon carbide paper of different grades (P600-grit, P1200-grit, and P2500-grit) and 3-µm alumina-based polishing compound were used to reduce the effect of surface roughness on fatigue life.

Three cyclic strain histories (see Fig. 1) were study: constant-amplitude, high-low sequences, and low-high sequences. The constant-amplitude tests were conducted under fully-reversed conditions with strain amplitudes between 0.5% and 2.75% (see Table 3). The high-low and low-high sequences included two steps of constant amplitude loading with a fix maximum strain. The higher step was symmetrical (i.e. $R_\varepsilon = -1$) while the other was asymmetrical (i.e. $R_\varepsilon \neq -1$). The first step was applied for a limited number of cycles (n_1) defined as 20% of the total fatigue life of the constant-amplitude loading case carried out at the same strain amplitude (see Table 3).

3. Numerical modelling and simulation

The simulation of cyclic plastic behaviour of the 7075-T651 aluminium alloy was done using a constitutive model based on the von Mises yield criterion coupled with a mixed isotropic-kinematic hardening law under an associated flow rule, as follows:

$$f(\sigma' - X) - Y \leq 0 \tag{1}$$

where $f(\sigma' - X)$ represents the von Mises yield criterion, σ' is the deviatoric Cauchy stress tensor, X is the backstress tensor (described by a non-linear kinematic hardening law) and Y is the yield stress (described by the isotropic hardening law). For the aluminium alloy, the yield stress was modelled using a Voce isotropic hardening law, i.e.

$$Y = Y_0 + (Y_{sat} - Y_0)[1 - \exp(-C_Y \bar{\varepsilon}^p)] \tag{2}$$

where Y_0, Y_{sat}, and C_Y are material parameters and $\bar{\varepsilon}^p$ is the equivalent plastic strain.

The non-linear kinematic hardening was modelled via an Armstrong-Frederick law:

$$\dot{X} = C_X \left[\frac{X_{sat}}{\overline{\sigma}}(\sigma' - X) - X\right] \dot{\overline{\varepsilon}}^p \tag{3}$$

where $\dot{X}$ is the backstress rate, C_X, and X_{sat} are material parameters, $\overline{\sigma}$ is the equivalent stress, and $\dot{\overline{\varepsilon}}^p$ is the equivalent plastic strain rate. The determination of the material constants that best described the cyclic elastic-plastic behaviour of both steels was carried out by minimising the function:

$$F(A) = \sum_{i=1}^{N} \left(\frac{\sigma^{Num}(A) - \sigma^{Exp}}{\sigma^{Exp}}\right)_i^2 \tag{4}$$

where $\sigma^{Num}(A)$ and σ^{Exp} are the analytical fitted and the experimentally measured values of true stress at point i (which corresponds to a given equivalent plastic strain value), N is the total number of experimental data points, and A is the set of material parameters to be identified. The fitting procedure was conducted using the data collected in the constant-amplitude loading tests for the different strain amplitudes (see Table 3) by applying a non-linear gradient-based optimisation algorithm [28~~3~~].

The finite element model used to simulate the saturated cyclic stress-strain behaviour of the tested alloy under strain-control mode consisted of a single 8-node three-dimensional isoparametric finite element (see Figure 2). Simulations were performed with the DD3IMP, an implicit three-dimensional finite element code developed at the University of Coimbra for the analysis of sheet metal forming processes [29~~4~~]. The cyclic loads were applied in four nodes located in the plane x = 1 mm along the direction parallel to the x-axis assuming 200 load sub-steps per cycle. Symmetry conditions were imposed in the planes x=0, y=0 and z=0.

Figure 3 compares the cyclic stress-strain response obtained in the experiments with that simulated numerically for a strain amplitude (ε_a) equal to 2.75% and a strain ratio (R_ε) equal to -1. In this figure, the cumulated plastic strain is plotted against the applied stress. The dash-dotted lines represent the simulations, while the dashed lines refer to the experiments. As can be seen, there is a very good agreement between the numerical results and the experimental data for the entire loading cycle. Overall, the elastic-plastic constitutive model captures well the cyclic stress-strain response of the tested alloy, either at the peak tensile stage or the peak compressive stage, which validates the proposed methodology.

4. Results and discussion

4.1 Cyclic stress-strain response

The cyclic stress-strain response of the tested alloy under constant-amplitude and step loading is summarised in Figure 4. Regarding the constant-amplitude tests, as can be seen, the material exhibited a mixed hardening-softening behaviour. At lower strain amplitudes, i.e. $\varepsilon_a \leq 1.00\%$, the cyclic response was characterised by strain-softening (see Fig. 4(a)). On the contrary, for strain amplitudes higher than 1.00%, it was observed a strain-hardening behaviour (see Fig. 4(b)). However, irrespective of the strain amplitude, the changes of the hysteresis loops during the tests were relatively small. This behaviour relatively independent from the load history can be explained by the face-centred cubic structure with high stacking fault energy which eases the cross slip during cyclic loading [2218].

Concerning the two-step variable-amplitude loading tests, as can be seen in Figure 4(c) and Figure 4(d), the cyclic stress-strain response of the higher steps is also quite stable, regardless of the loading sequence. Under lower strain amplitudes, the variations of the hysteresis loops are more expressive, which can be explained by the mean stress effect since these steps are not symmetrical. It is also clear that the peak compressive stresses tend to decrease with the increase of the loading cycles, either for the high-low sequence or the low-high sequence. Nevertheless, the peak tensile stresses behave differently, maintaining a constant value during the test for both loading sequences.

The transient behaviour associated with the cyclic response in strain control can be better analysed using dependent parameters. Figure 5(a) plots the stress amplitude against the number of cycles for different constant-amplitude and step loading tests. Regarding the constant-amplitude loading tests, we can see a mixed softening-hardening behaviour. At higher strain amplitude, i.e. ε_a = 1.25%, the softening response is characterised by a small reduction of stress amplitude during the first cycles followed by a slight increase until a saturated-like stage is reached. At lower strain amplitude, i.e. ε_a = 0.70%, hardening is observed throughout the entire lifetime. In the first few cycles, the hardening degree is higher. After this initial stage, the increase of stress amplitude is tenuous until the final failure.

Concerning the step loading tests, the stress responses are similar to those observed for constant-amplitude loading during most of the test. For the highest level of the high-low sequence, the stress amplitude is basically similar to that of the case conducted under constant-amplitude, which is expected since the loading scenarios are similar. However, when the second step starts, which is an asymmetrical one, the stress amplitude suddenly moves away from the values of the case conducted under constant-amplitude and then the material strain-hardens during a short initial period. After this period, the curves of the constant-amplitude and step loading tests tend to overlap.

As far as the low-high sequence is concerned, the response at the lowest level, which is characterised by an asymmetrical pattern, is slightly different from that of the case conducted at the same strain amplitude with R_ε = -1. The degree of strain-hardening of this first step is clearly smaller. In the second step, which is symmetrical, the values of stress amplitude sudden increase, denoting a strain-hardening response. After that, there is a progressive reduction until the final failure. It is also interesting to note that the values of stress amplitude are relatively close to those of the case tested under fully-reversed constant-amplitude loading. Moreover, the fatigue lives of both step loading tests are similar to each other and are between those obtained at constant amplitude for the higher and the lower strain amplitudes.

The hysteresis loop development during the test is another important aspect under strain-control mode. Based on the previous analysis, it can be hypothesised that the shape variations are not particularly expressive for this alloy. Figure 5(b) shows the variation of the plastic strain energy density per cycle (ΔW_p) with the number of cycles for constant-amplitude and step loading sequences. Overall, at the highest strain amplitudes, irrespective of the loading scenario, the values of plastic strain energy density per cycle are constant throughout the test. Nevertheless, at the lowest strain amplitudes, there is a small reduction of ΔW_p with the number of cycles, particularly at the first stage of the tests.

Under non-zero mean strain ($R_\varepsilon \neq$ -1), i.e. at the lowest strain levels of the step loading tests, mean stress relaxation phenomena were observed. The variation of mean stress with the number of cycles for different loading histories is exhibited in Figure 6(a). The degree of mean stress relaxation is higher at the beginning of the lowest strain level, either for high-low or low-high sequence, and then tends to a constant value. It is well-known that the mean stress relaxation gradients of a specific material are not only associated with the strain ratio, but also with the strain amplitude. In general, high-strength aluminium alloys relax more rapidly at higher strain amplitudes and at higher strain ratios [141-153]. The same trends were observed for the 7075-T651 aluminium alloy.

In relation to the highest strain levels of the two-step sequences, the mean stress values were close to zero during the entire lifetime, which is expected since such tests were conducted under fully-reversed conditions (see Figure 6(a)). In addition, these mean stress values were quite close to those found for constant-amplitude loading. In all cases, the stress values are slightly negative, which may be justified by the use of the nominal cross-section area in the calculation of both the maximum and minimum stresses. It is also interesting to note that the asymmetrical steps (R_ε = -0.12 and ε_a = 0.70%) do not fully relax, due to insufficient plastic strain in each cycle. This fact has been reported for other aluminium alloys [14~~2~~,30~~25~~].

The mean stress relation is likely to affect the position of the hysteresis loops with respect to the abscissa axis. The ratio of positive elastic strain energy density per cycle to the negative elastic strain energy density per cycle ($\Delta W_{e+}/\Delta W_{e-}$) can be used to investigate such variation. Figure 6(b) displays the variation of the $\Delta W_{e+}/\Delta W_{e-}$ ratio with the number of cycles for different loading histories, namely high-low sequence, low-high sequence, and constant-amplitude. Not surprisingly, under fully-reversed conditions, this ratio is close to unity, indicating a reasonable symmetry regarding the zero-stress coordinate line. On the other hand, it is also clear that the values of the $\Delta W_{e+}/\Delta W_{e-}$ ratio under fully-reversed conditions are similar, either for the constant-amplitude or the step loading tests.

In contrast, under non-zero mean strain, the above-mentioned ratio significantly deviates from unity, regardless of the loading sequence, as can be seen in Figure 6(b). There is a progressive change during the lifetime towards a stable value. Furthermore, the degree of relaxation is clearly dependent on the loading scenario, i.e. the lowest step of the high-low sequence ($\varepsilon_{a,1}$ = 1.25% and $\varepsilon_{a,2}$ = 0.70%) leads to more significant relaxation rates than that of the low-high sequence ($\varepsilon_{a,1}$ = 0.70% and $\varepsilon_{a,2}$ = 1.25%). Another important conclusion is that the $\Delta W_{e+}/\Delta W_{e-}$ ratio can better capture the asymmetries of the hysteresis loop shapes than the mean stress, which is an interesting outcome.

4.2 Stable response and fatigue lifetime

The stable stress-strain response of the tested alloy under fully-reversed conditions was examined from the mid-life hysteresis loops. Figure 7 compares the recorded shapes at different strain amplitudes with those simulated using the numerical model described in Section 3. For the sake of comparability, the compressive tips of the hysteresis loops are made to coincide. In general, as can be seen in the figure, experimental results and numerical simulations are in good agreement, particularly for the upper branches. Concerning the lower branches, we can identify more significant differences, but still close to the experimental cyclic response, which validates the proposed methodology.

It is also interesting to note that the upper branches of the hysteresis loops do not follow a unique curve. This demonstrates that the 7075-T651 aluminium alloy does not exhibit a Masing-type behaviour. Masing materials are those for which the upper branches of the hysteresis loops obtained at different strain amplitudes coincide when the lower tips are moved to a common origin which corresponds to the maximum compressive stress (see Figure 7). The violation of the Masing behaviour is attributed to an insufficient elastic region of the hysteresis loops, generally associated with the dislocation density and the cell size [3126]. In the literature, there are several examples of aluminium alloys identified as non-Masing materials [142,3126-3328].

The strain-life curves obtained from the fully-reversed constant-amplitude fatigue tests are displayed in Figure 8(a). In the studied range, as can be seen in the figure, the plastic strain versus life and the elastic strain versus life relationships were successfully fitted by linear functions. It was also observed that the fitted functions correlated very well with the results available in the literature (see black markers) for this aluminium alloy [3429]. On the other hand, it can also be concluded that the strain-life data points computed from the hysteresis loops simulated numerically are in good agreement with those determined in the experiments. The more relevant differences occurred for the lowest strain amplitudes.

Figure 8(b) plots both the plastic strain energy density per cycle (ΔW_p) versus life relationship and the total strain energy density per cycle (ΔW_t) versus life relationship determined from the experimental hysteresis loops collected from the constant-amplitude fatigue tests. A linear function was found to better represent the $\Delta \mathrm{W_p}$-life relationship. The tensile elastic energy at the material fatigue limit (ΔW_{0t}) of the $\Delta \mathrm{W_t}$-life relationship was estimated for 1×10^6 cycles. Regarding the energy-life data points obtained from the simulated hysteresis loops, no relevant differences were observed when compared to the experimental results.

The accurate simulation of the saturated hysteresis loops under fully-reversed conditions, as demonstrated above, opens interesting perspectives to the development of an robust fatigue life prediction model. However, it is still needed to investigate the hysteresis loop shapes obtained for the asymmetrical loading scenarios. A comparison for four different cases is presented in Figure 9. The dashed lines represent the loops simulated with the proposed approach, while the full lines correspond to the mid-life cycle of the lowest strain level (i.e. $R_\varepsilon \neq$ -1) of the high-low loading sequences.

As can be seen in the above-mentioned figure, the numerical and the experimental stress-strain responses are rather similar, particularly for the tensile tips, which are perfectly overlapped, irrespective of the strain amplitude or the strain ratio. With regard to the compressive tips, the conclusions are slightly different. The points are also overlapped for lower strain amplitudes, but they slightly deviate for higher strain amplitudes. Nevertheless, in any case, we can consider that the extreme points are close to each other. Thus, it makes possible the development of a robust fatigue life prediction model, provided that an adequate fatigue damage accumulation law is considered.

4.3 Fatigue life prediction

Fatigue life predictions were performed using three well-known models sensitive to mean stress in conjunction with a linear damage accumulation law. The models are based on the Coffin-Manson (CM), Smith-Watson-Topper (SWT), and Total Strain Energy Density (TSED) parameters. The damage accumulation law is based on the Palmgren-Miner damage rule. The three models as well as the linear damage accumulation rule are described below.

The Coffin-Manson (CM) model, with the mean stress correction of the elastic term introduced by Morrow, can be written as follows [35~~0~~-36~~1~~]:

$$\varepsilon_a = \frac{\left(\sigma_f' - \sigma_m\right)}{E}\,(2\mathrm{N_f})^b + \varepsilon_f'\,(2\mathrm{N_f})^c \tag{5}$$

where ε_a is the strain amplitude, σ_f' is the fatigue strength coefficient, b is fatigue strength exponent, ε_f' is the fatigue ductility coefficient, c is the fatigue ductility exponent, and σ_m is the mean stress.

The model based on the Smith-Watson-Topper (SWT) parameter is usually defined by the following formula [37~~2~~]:

$$\varepsilon_a\,\sigma_{max} = \frac{\left(\sigma_f'\right)^2}{E}\,(2\mathrm{N_f})^{2b} + \sigma_f'\,\varepsilon_f'\,(2\mathrm{N_f})^{b+c} \tag{6}$$

where ε_a and σ_{max} are, respectively, the strain amplitude and the maximum stress, σ_f' is the fatigue strength coefficient, b is the fatigue strength exponent, ε_f' is the fatigue ductility coefficient, c is the fatigue strength exponent, and E is Young's modulus.

The total strain energy density (TSED) is another fatigue quantifier often used to account for mean stress effects [383]:

$$\Delta W_t = \kappa_t \, (2N_f)^{\alpha_t} + \Delta W_{0t} \tag{7}$$

where κ_t and α_t are material constants, and ΔW_{0t} is the tensile elastic energy at the material fatigue limit. Here, it is defined by the sum of both the elastic positive strain energy density per cycle, and the plastic strain energy density per cycle (see Figure 6(b)).

The cumulative fatigue damage was calculated using the Palmgren-Miner damage rule. For two-step loading conditions, it leads to [186-20]:

$$\frac{n_1}{N_1} + \frac{n_2}{N_2} = 1 \tag{8}$$

where n_1 and n_2 are the number of cycles applied at the first and the second strainess levels, respectively; and N_1 and N_2 are the fatigue life at the first and the second strainess level.

Predicted fatigue lives versus observed fatigue lives for the studied loading histories, computed from the three fatigue models in conjunction with the cumulative damage rule, are presented in Figure 10. In this first analysis, the fatigue variables (i.e. strain amplitude, mean stress, maximum stress, SWT-damage parameter, and total strain energy density) were computed from the mid-life hysteresis loops obtained experimentally. As can be seen in the figure, the CM-based and the SWT-based results show a close correlation between the fatigue life and the loading history, either for the high-low sequence or the low-high sequence. On the contrary, the TSED-based approach is less accurate, leading to unsatisfactory results in some cases.

It is worth to note that the predictions based on the SWT parameter fall within a narrow range, and are tendentially conservative, which is another interesting finding. In the case of the CM-based model, although the data points are also well correlated, they are spread in a wider range, and are either conservative or non-conservative. These results clearly demonstrate that both the CM-based and the SWT-based approaches, in conjunction with the Palmgren-Miner linear damage rule, can appropriately capture the effect of load sequence on fatigue behaviour for the tested aluminium alloy under two-step loading.

Since the simulated hysteresis loops are close to the experimental ones, it is reasonable to admit that the fatigue life predictions based on the numerical simulations of the cyclic stress-strain response are likely to be sufficiently robust. The predicted fatigue lives and the observed fatigue lives computed from the simulated hysteresis loops, using the CM-based and the SWT-based models, are compared in Figure 11. In this approach, the fatigue variables (i.e. strain amplitude, mean stress, and maximum stress) were determined from the numerically simulated loops. For the sake of comparability, the data points corresponding to the experimental-based approach (i.e. those plotted in Figure 10) are represented in grey.

As can be seen in the above-mentioned figure, the quality of results computed by means of the proposed strategy ~~are~~ is relatively similar to those obtained from the experimental hysteresis loops, either for the CM-based model, or the SWT-based model. In general, we can see that the data points are slightly less conservative. However, there is a good correlation between the calculated fatigue lives and the observed fatigue lives for both models, irrespective of the loading sequence. Particularly for the SWT-based model, the results are within scatter bands of factors of 1.5 and most of them evidence a very low scatter. This demonstrates that the numerical-based approach is sensitive to the load sequence effect.

In order to better evaluate the predictive capabilities of the tested approaches, a statistical study based on the probability density functions of the prediction error was carried out. Here the prediction error (P_E) was defined by the following formula:

$$P_E = \text{Log}\,(N_e) - \text{Log}\,(N_p) \tag{9}$$

where N_e is the experimentally observed fatigue life, and N_p is the predicted fatigue life. More accurate models are generally associated with lower standard deviations and mean errors close to zero. As hypothesised above, the SWT-based models better capture the load sequence effects on fatigue behaviour than the CM-based models because the mean errors are closer to zero and the standard deviations are smaller. Moreover, it can be observed that the numerical approaches are more shifted to the non-conservative side than the experimental ones. Apart from that, the probability density functions are relatively similar.

To conclude this section, we would like to emphasise that the proposed numerical tool is capable of capturing the effect of loading history on the fatigue behaviour of the 7075-T651 aluminium alloy under two-step loading sequences. It only requires a simple strain-life curve and an elastic-plastic constitutive model, which can be met by a series of standard fully-reversed strain-controlled tests. Therefore, the predictive approach is simplified, since a limited number of fatigue tests is necessary, and ultimately the cost and time associated with the calculations are significantly reduced. Last but not least, the proposed numerical tool is suitable for industrial application.

5. Conclusions

The paper studied the load sequence effect on cyclic deformation and fatigue behaviour of 7075-T651 aluminium alloy under two-step variable-amplitude loading. High-low and low-high sequences, encompassing both symmetrical and asymmetrical steps, were performed under strain-controlled mode for different loading scenarios. The stabilised stress-strain response was simulated numerically using an elastic-plastic constitutive model. Fatigue life was predicted by combining a linear damage accumulation rule with the CM-based, SWT-based, and TSED-based parameters. The following conclusions can be drawn:

- A constitutive model based on the von Mises yield criterion coupled with a mixed isotropic-kinematic hardening has been adequate to simulate the stabilised stress-strain response of the tested alloy under strain-control mode for symmetrical and asymmetrical loading cases;
- Under fully-reversed strain-controlled materials, the material exhibited a mix cyclic hardening-softening behaviour. It hardened for strain amplitudes higher than 1.0% and exhibited a softening response below this value. However, the changes of the hysteresis loops were relatively small;
- In the two-step loading cases, a hardening behaviour was observed during a short initial period, when the second step was applied. After this period, the responses under

constant- and twovariable-step loadingamplitude were similar. The degree of strain-hardening was affected by the load sequence;

- Mean stress relaxation was also affected by the load sequence. Higher mean stress relaxation rates were observed in the beginning of the asymmetrical steps. Moreover, high-low sequences led to higher mean stress relaxation rates than the low-high sequences;
- The linear damage accumulation rule in conjunction with the SWT damage parameter provided better fatigue life predictions than the models based on the strain-life and energy-life relationships. This was attributed to the fact that this fatigue quantifier includes stress and strain terms, making it more sensitive to load sequence effects.
- Fatigue life predictions computed from the hysteresis loops simulated numerically using the CM-based and the SWT-based models were close to those obtained from the experimental hysteresis loops. The latter led to better life predictions with all points within scatter bands of factors of 1.5.

Acknowledgements

This research is sponsored by FEDER funds through the program COMPETE – Programa Operacional Factores de Competitividade – and by national funds through FCT – Fundação para a Ciência e a Tecnologia – under the project UIDB/00285/2020.

References

1. Ashkenazi D (2019). How aluminum changed the world: a metallurgical revolution through technological and cultural perspectives. Technological Forecasting and Social Change 143, 101–13.
2. Zhang X, Chen Y, Hu J (2018). Recent advances in the development of aerospace materials. Progress in Aerospace Sciences 97, 22–34.
3. Carpinteri A, Vantadori S, Łagoda T, Karolczuk A, Kurek M, Ronchei C (2018). Fatigue assessment of metallic components under uniaxial and multiaxial variable amplitude loading. Fatigue and Fracture of Engineering Materials and Structures 41, 1306-1317.
4. Zhu SP, Liao D, Liu Q, Correia JAO, Jesus AMP (2020). Nonlinear fatigue damage accumulation: Isodamage curve-based model and life prediction aspects. International Journal of Fatigue Volume 128, 105185
5. Vantadori S, Carpinteri A, Fortese G, Ronchei C, Scorza D, Zanichelli A (2018). Fatigue lifetime evaluation of notched components: Implementation of the control volume

concept in a strain-based LCF criterion. Theoretical and Applied Fracture Mechanics 97, 400-408.

6. Liao D, Zhu SP, Correia JAFO, De Jesus AMP, Berto F (2020). Recent advances on notch effects in metal fatigue: A review. Fatigue and Fracture of Engineering Materials and Structures 43, 637-659.

7. Negru R, Şerban DA, Marşavina L, Magda A (2016). Lifetime prediction in medium-cycle fatigue regime of notched specimens. Theoretical and Applied Fracture Mechanics 84, 140-148.

~~6.~~8. Zakaria KA, Abdullah S, Ghazali MJ (2016). A review of the loading sequence effects on the fatigue life behaviour of metallic materials. Journal of Engineering Science and Technology Review 9, 189-200.

~~7.~~9. Marciniak Z, Rozumek D, Macha E (2008). Fatigue lives of 18G2A and 10HNAP steels under variable amplitude and random non-proportional bending with torsion loading. International Journal of Fatigue 30, 800-813.

~~8.~~10. Necemer B, Zupanic F, Gabriel D, Tarquino E, Sraml M, Glodez S (2021). Low cycle fatigue behaviour of ductile aluminium alloys using the inelastic energy approach. Materials Science and Engineering A 800, 140385."

~~9.~~11. Long XY, Branco R, Zhang FC, Berto F, Martins RF (2020). Influence of Mn addition on cyclic deformation behaviour of bainitic rail steels. International Journal of Fatigue 132, 105362.

12. Koh SK, Oh SJ, Li C, Ellyin F (1999). Low-cycle fatigue life of SiC-particulate-reinforced Al-Si cast alloy composites with tensile mean strain effects. International Journal of Fatigue 21, 1019–1032.

~~10.~~13. Linul E, Serban DA, Marsavina L, Kovacik J (2016). Low-cycle fatigue behaviour of ductile closed-cell aluminium alloy foams. Fatigue and Fracture of Engineering Materials and Structures 40, 597-604.

~~11.~~14. Branco R, Costa JD, Borrego LP, Wu SC, Long XY, Zhang FC (2019). Effect of strain ratio on cyclic deformation behaviour of 7050-T6 aluminium alloy. International Journal of Fatigue 129, 105234.

~~12.~~15. Sandor BI. Fundamentals of cyclic stress and strain. University of Wisconsin Press; 1972, ISBN: 978-0299061005.

~~13.~~16. Hectors K, Waele W (2021). Cumulative damage and life prediction models for high-cycle fatigue of metals: a review. Metals 11, 204.

14.17. Fatemi A, Yang L (1998). Cumulative fatigue damage and life prediction theories: a survey of the state of the art for homogeneous materials. International Journal of Fatigue 20, 9-34

18. Miner MA (1954). Cumulative damage in fatigue. Journal of Applied Mechanics 67, AI59-AI64.

19. Zhu SP, Hao Y-Z, Correia JAFO, Lesiuk G, Jesus AMP (2019). Nonlinear fatigue damage accumulation and life predictionof metals: A comparative study. Fatigue and Fracture of Engineering Materials and Structures 42, 1271-1282.

15.20. Lv Z, Huang H-Z, Zhu S-P, Gao H, Zuo F (2015). A modified nonlinear fatigue damage accumulation model. International Journal of Damage Mechanics 24(2), 168–181.

21. Topper TH, Sandor BI, Morrow J (1969). Cumulative fatigue damage under cyclic strain control. Journal of Materials 4, 189–199.

16.22. Colin J, Fatemi A (2010). Variable amplitude cyclic deformation and fatigue behaviour of stainless steel 304L including step, periodic, and random loadings. Fatigue and Fracture of Engineering Materials and Structures 33, 205-220.

17.23. Zhao X, Li H, Chen T, Cao B, Li X (2019). Mechanical properties of aluminum alloys under low-cycle fatigue loading. Materials 12, 2064.

24. Cunha J, Mateus A, Malça C, Costa J, Branco R (2021). Effect of Strain Load History on Fatigue Behaviour of the 7075-T651 Aluminium Alloy. Sustainability and Automation in Smart Constructions. Advances in Science, Technology & Innovation, pages 279-284, Springer.

18.25. S.P. Zhu, Q. Lei, Q.Y. Wang (2017) Mean stress and ratcheting corrections in fatigue life prediction of metals. Fatigue and Fracture of Engineering Materials and Structures 40(9), 1343-1354.

19.26. Agius D, Kourousis K, Wallbrink C (2018). A modification of the multicomponent Armstrong–Frederick model with multiplier for the enhanced simulation of aerospace aluminium elastoplasticity. International Journal of Mechanical Sciences 144, 118–133.

20.27. Nath A, Barai S, Ray K (2019). Prediction of asymmetric cyclic-plastic behaviour for cyclically stable non-ferrous materials. Fatigue and Fracture of Engineering Materials and Structures 42, 2808–2822.

21.28. Lasdon LS, Waren AD, Jain A, Ratner MW. Design and testing of a generalized reduced gradient code for nonlinear optimization. NTIS National Technical Information Service U. S. Department of Commerce, Cleveland. 1975.

~~22.~~29. Oliveira MC, Alves JL, Menezes LF (2008). Algorithms and strategies for treatment of large deformation frictional contact in the numerical simulation of deep drawing process. Archives of Computational Methods in Engineering 15, 113–162.

~~23.~~30. Hao H, Ye D, Chen C (2014). Strain ratio effects on low-cycle fatigue behavior and deformation microstructure of 2124–T851 aluminum alloy. Materials Science and Engineering A 605, 151–159.

~~24.~~31. Plumtree A, Abdel-Raouf HA (2001). Cyclic stress–strain response and substructure. International Journal of Fatigue 23, 799–805.

~~25.~~32. Rusk DT, Taylor RE, Hoffman PC (2006). Testing of 7050-T7451 aluminium strain-life coupons for a probabilistic strain-life curve. Department of the Navy Naval Air Warfare Center Aircraft Division, Maryland, Report NAWCADPAX/TR-2006/140.

~~26.~~33. Branco R, Costa JD, Borrego LP, Wu SC, Long XY, Antunes FV (2020). Effect of tensile pre-strain on low-cycle fatigue behaviour of 7050-T6 aluminium alloy. Engineering Failure Analysis 114, 104592.

~~27.~~34. Zhao T, Jiang Y (2008). Fatigue of 7075-T651 aluminum alloy. International Journal of Fatigue 30, 834–849.

~~28.~~35. Manson SS (1954). Beahaviour of materials under conditions of thermal stress. NACA TN-2933, National Advisory Committee for Aeronautics.

~~29.~~36. Morrow JD (1965). Cyclic plastic strain energy and fatigue of metals. International Friction, Damping and Cyclic Plasticity, American Society for Testing and Materials, ASTM STP 378, Philadelphia, 45-87.

~~30.~~37. Smith R, Watson TH, Topper T (1970). A stress-strain parameter for the fatigue of metals. Journal of materials JMLSA 5, 767–778.

~~31.~~38. Golos K, Ellyin F (1988). A total strain energy density theory for cumulative damage. Journal of Pressure Vessel Technology 110, 36–41.

Tables

Table 1. Nominal chemical composition of the 7075-T651 aluminium alloy (wt.%)

Zn	Mg	Cu	Si	Fe	Mn	Al
4.89	2.12	1.52	0.33	0.007	0.09	Balance

Table 2. Mechanical properties of the tested 7075-T651 aluminium alloy

Young's modulus, E (GPa)	71.7
Yield strength, σ_{YS} (MPa)	503
Ultimate tensile strength, σ_{UTS} (MPa)	561
Poisson's ratio, ν	0.306
Elongation at break (%)	11

Table 3. Summary of constant-amplitude (CA) and high-low (HL) and low-high (LH) tests

Sequence	$\varepsilon_{a,1}$ (%)	$R_{\varepsilon,1}$	$\varepsilon_{a,2}$ (%)	$R_{\varepsilon,2}$	n_1 (cycle)	n_2 (cycle)	N_f (cycle)
CA	0.50	-1	-	-	11084	-	11084
CA	0.70	-1	-	-	1325	-	1325
CA	0.80	-1	-	-	609	-	609
CA	1.00	-1	-	-	302	-	302
CA	1.25	-1	-	-	167	-	167
CA	1.50	-1	-	-	119		119
CA	1.75	-1	-	-	115	-	230
CA	2.25	-1	-	-	56	-	56
CA	2.75	-1	-	-	34	-	34
HL	1.50	-1	0.70	0.07	24	861	885
HL	1.25	-1	0.70	-0.12	33	559	592
HL	1.00	-1	0.70	-0.40	68	637	705
HL	1.50	-1	0.50	0.33	24	2893	2917
HL	1.25	-1	0.50	0.20	33	2091	2124
HL	1.00	-1	0.50	0	68	3719	3787
LH	0.70	0.07	1.50	-1	265	117	382
LH	0.70	-0.12	1.25	-1	265	150	415
LH	0.70	-0.40	1.00	-1	265	267	532
LH	0.50	0.33	1.50	-1	2216	48	2264
LH	0.50	0.20	1.25	-1	2216	26	2242
LH	0.50	0	1.00	-1	2216	319	2535

Figures

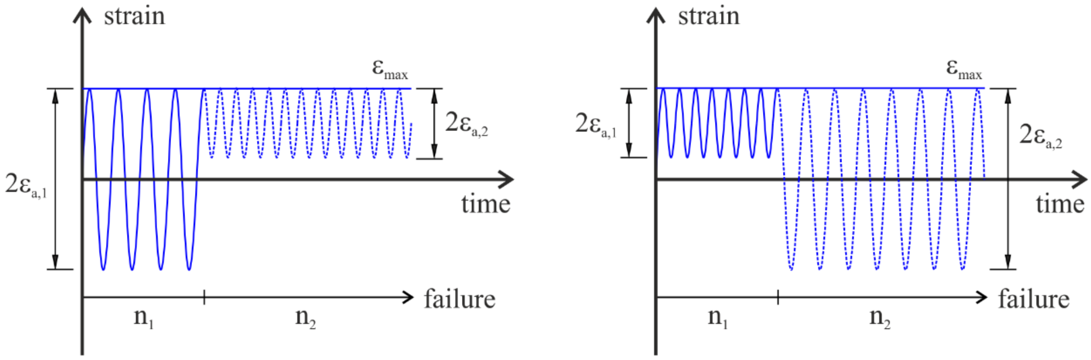

Figure 1. Cyclic loading histories: (a) high-low sequence; and (b) low-high sequence ($2\Delta\varepsilon_{a,1}$ and $2\Delta\varepsilon_{a,2}$ represent the strain ranges of step 1 and step 2, respectively; n_1 and n_2 represent the number of cycles applied in step 1 and step 2, respectively.

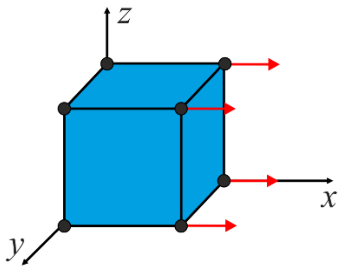

Figure 2. Finite element model used to simulate the saturated cyclic stress-strain response of the 7075-T651 aluminium alloy under strain-controlled conditions.

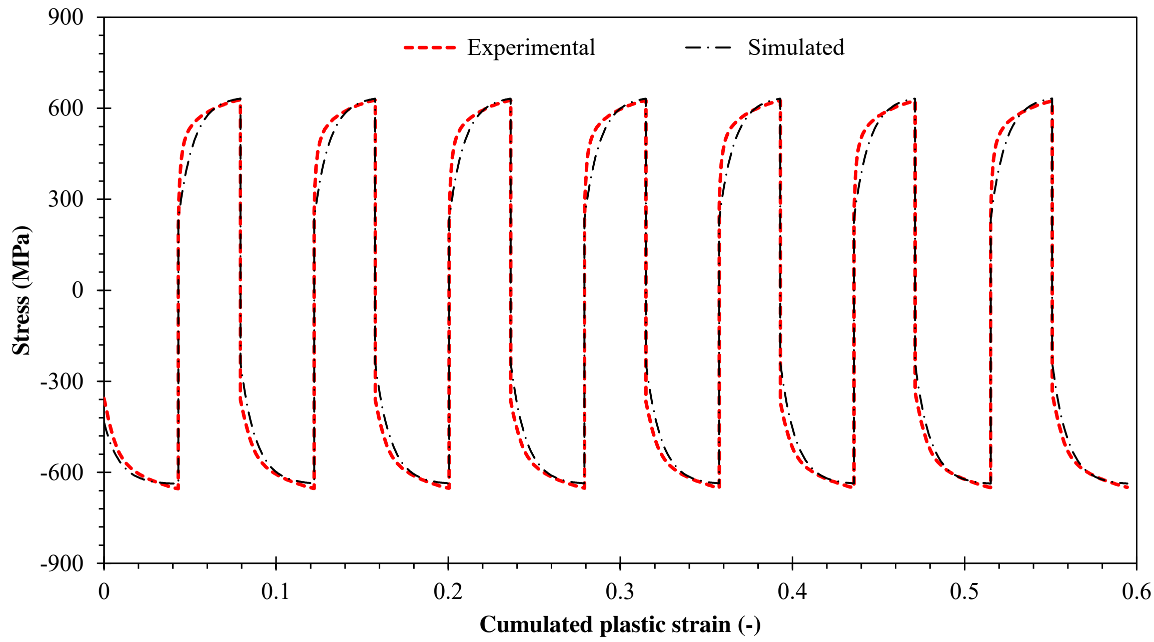

Figure 3. Numerical and experimental cyclic stress-~~stress~~ strain responses of the 7075-T651 aluminium alloy under strain-controlled conditions at ε_a = 2.75% and R_ε = -1.

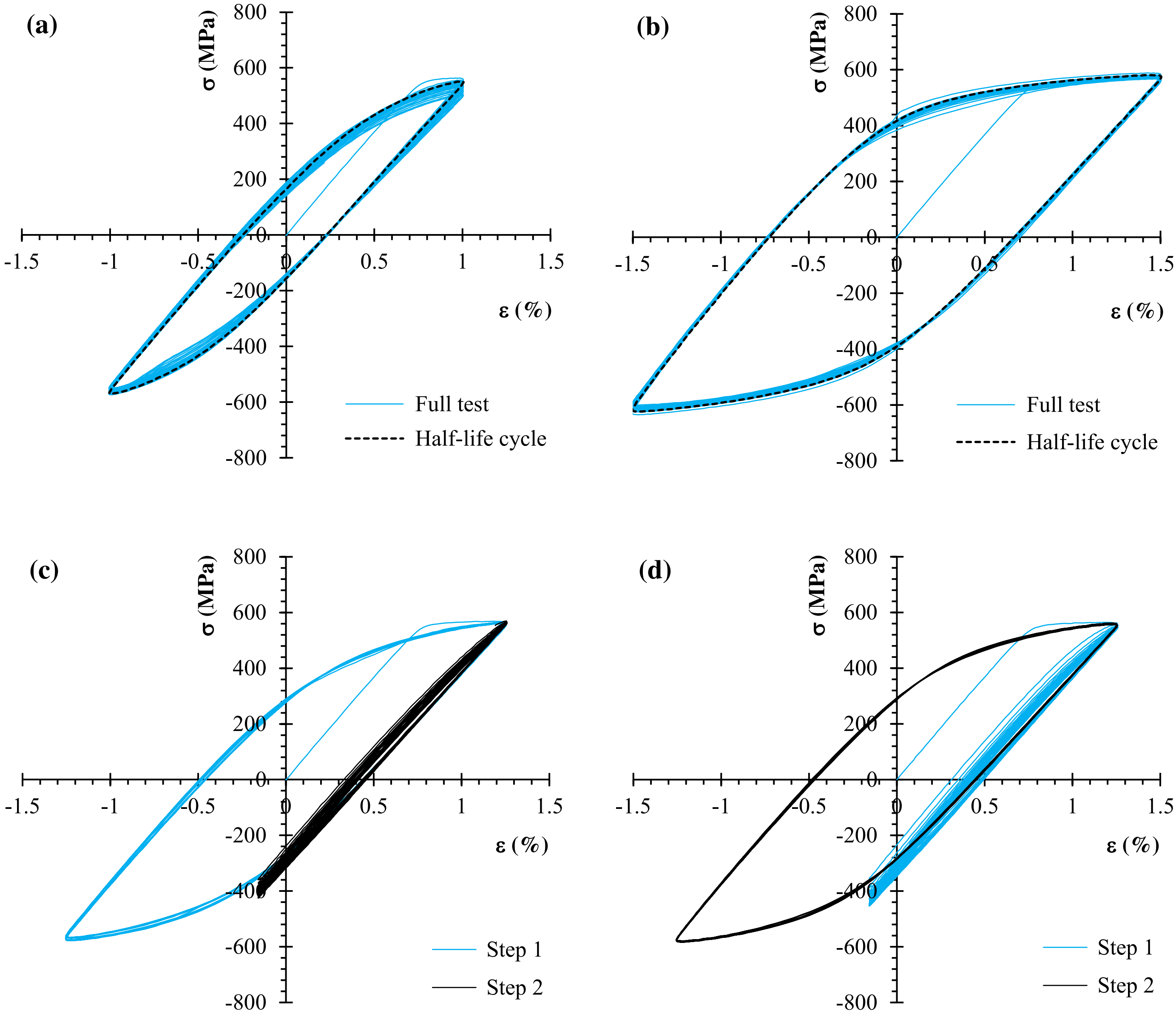

Figure 4. Cyclic hysteretic response of the 7075-T651 aluminium alloy under strain-controlled conditions: (a) constant-amplitude loading with ε_a = 1.00%; (b) constant-amplitude loading with ε_a = 1.25%; (c) high-low step loading with $\varepsilon_{a,1}$ = 1.25% and $\varepsilon_{a,2}$ = 0.70%; and (d) low-high step loading with $\varepsilon_{a,1}$ = 0.70% and $\varepsilon_{a,2}$ = 1.25%.

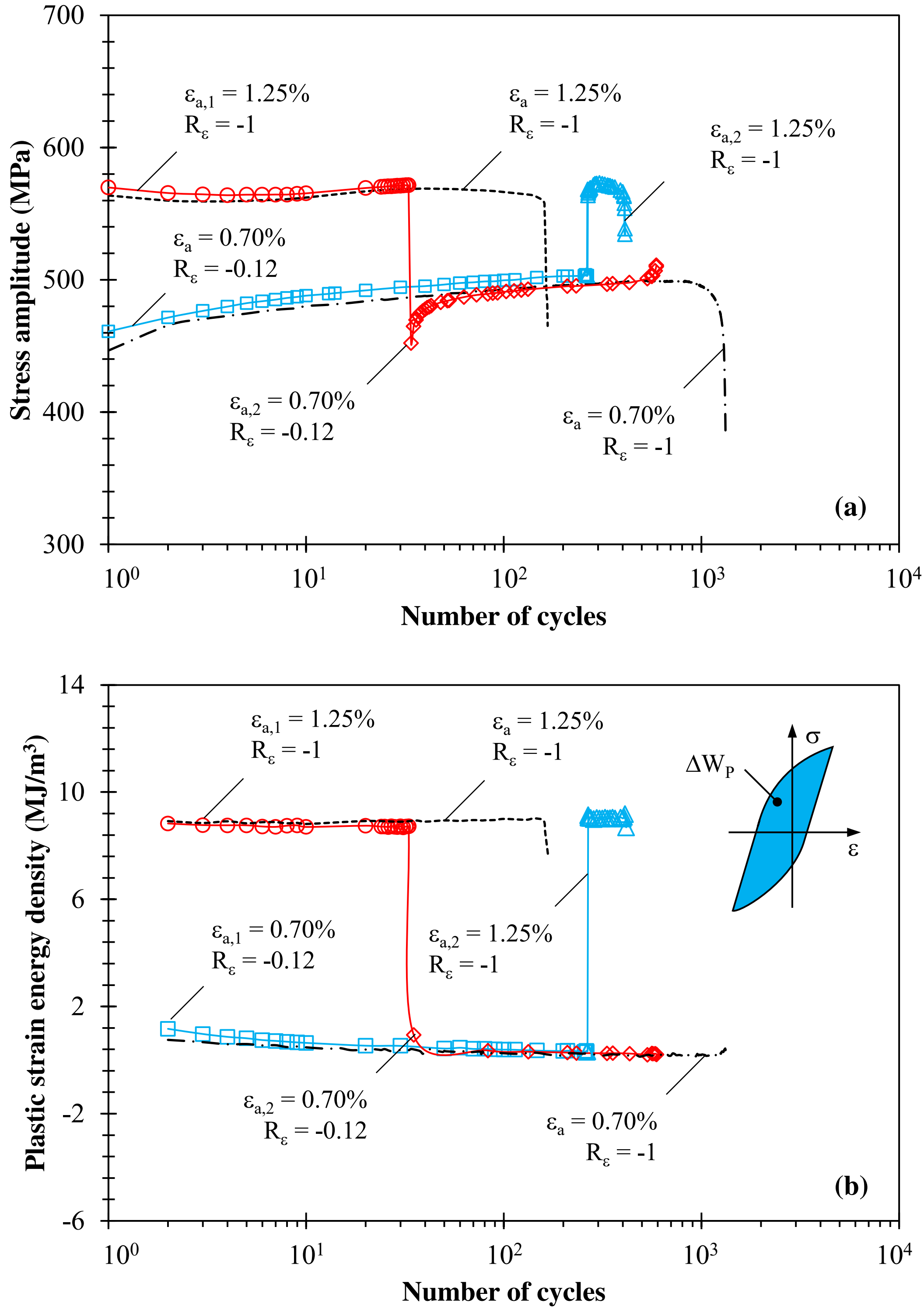

Figure 5. (a) Stress ~~range~~ amplitude versus number of cycles; and (b) plastic strain energy density versus number of cycles.

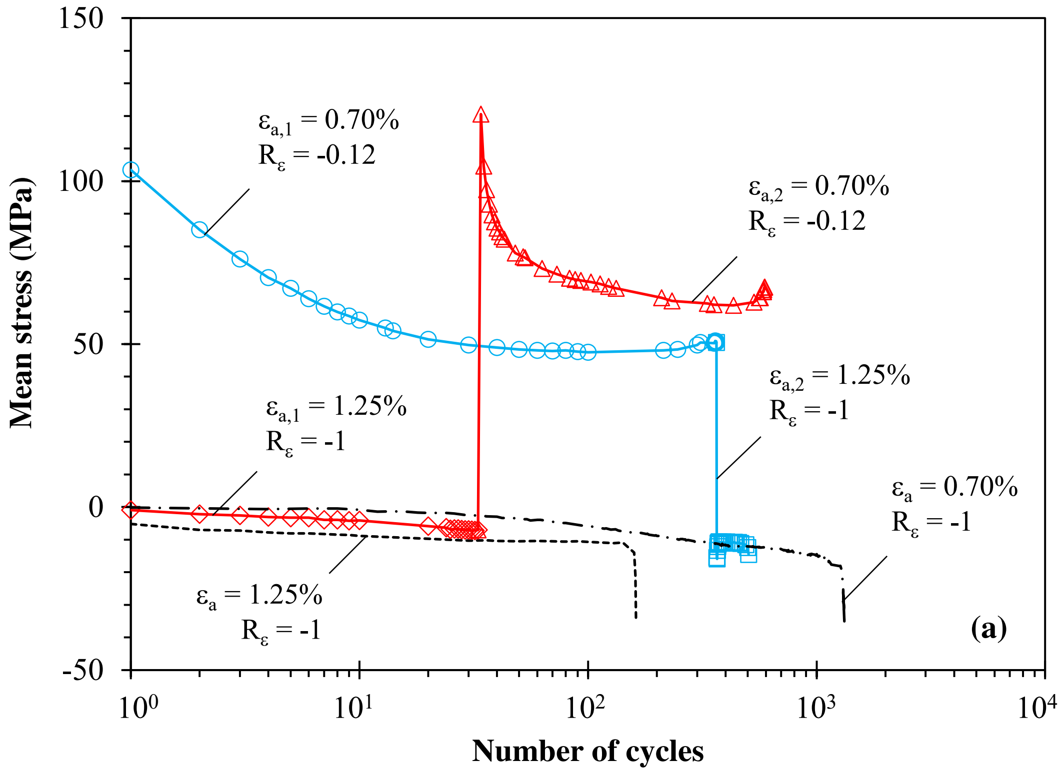

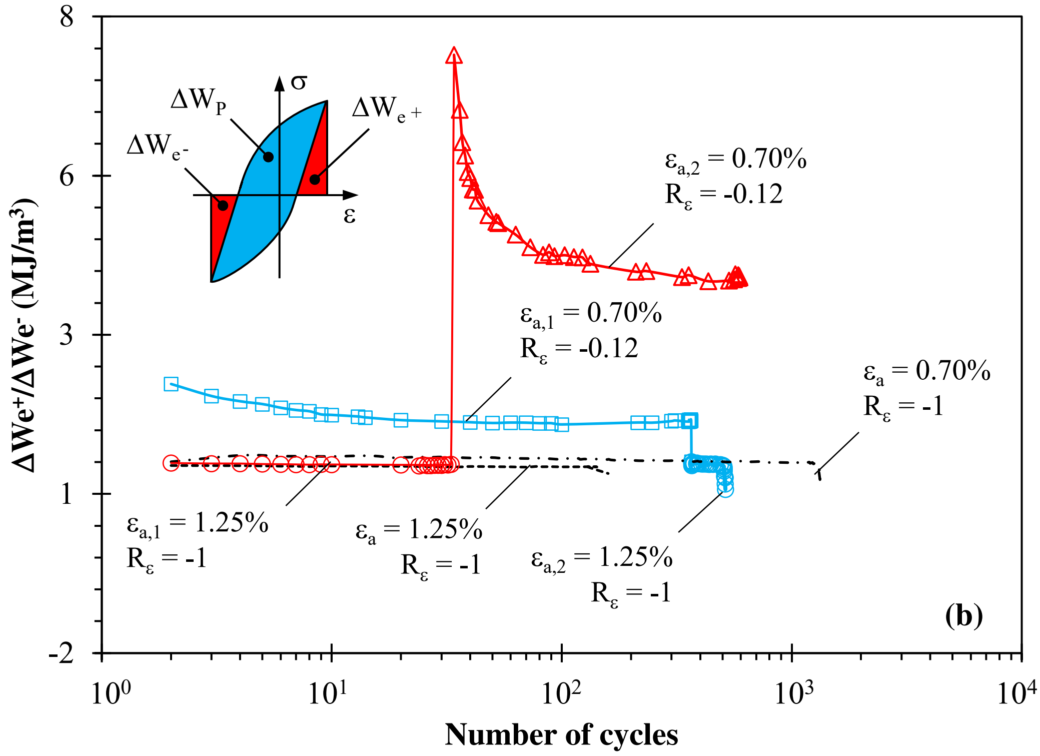

Figure 6. (a) Mean stress versus number of cycles; and (b) $\Delta W_{e+}/\Delta W_{e-}$ ratio versus number of cycles.

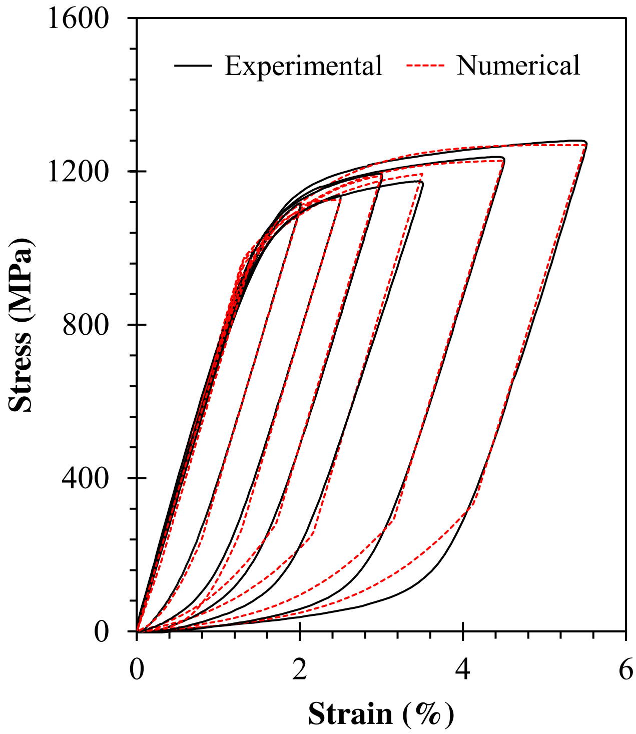

Figure 7. Comparison of experimental and numerical stable hysteresis loops, in relative coordinates, obtained under constant-amplitude loading tests. Experimental testes refer to the mid~~half~~-life cycle.

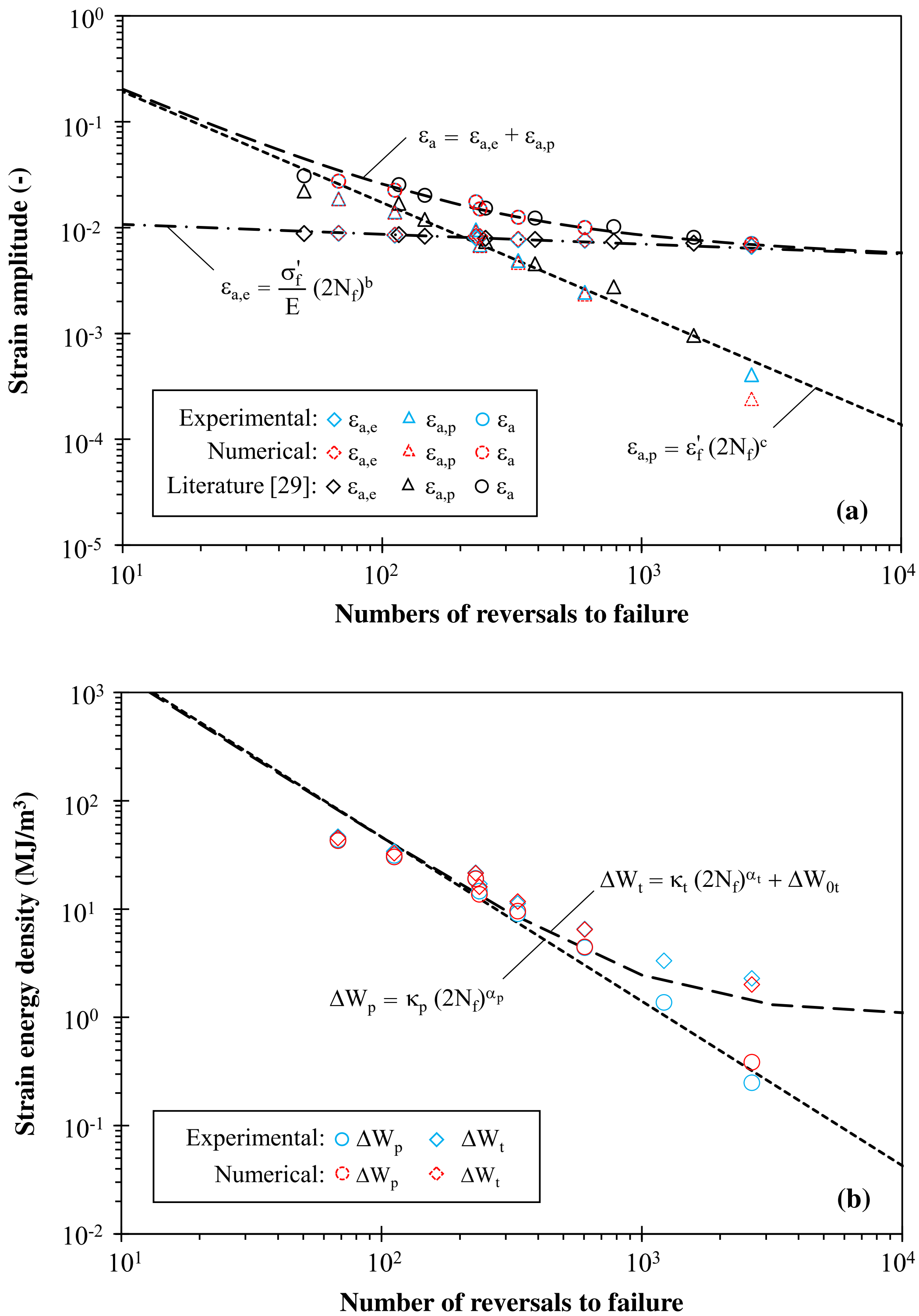

Figure 8. Strain-life curve (a) and energy-life curve (b) of the tested aluminium alloy under fully-reversed strain controlled conditions. Dashed lines represent the fitted functions determined from the experimental data.

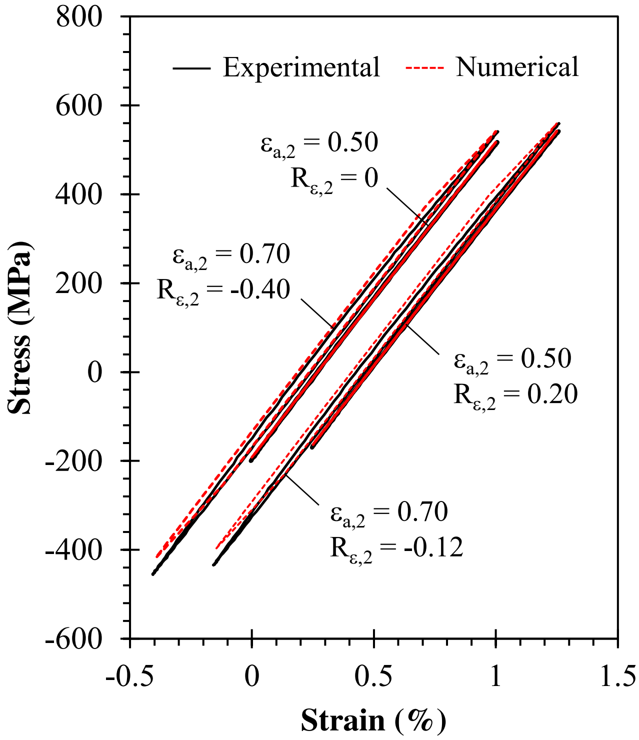

Figure 9. Comparison of experimental and numerical hysteresis loops obtained in the high-low tests for the asymmetrical steps. Experimental tests refer to the mid-life cycle.

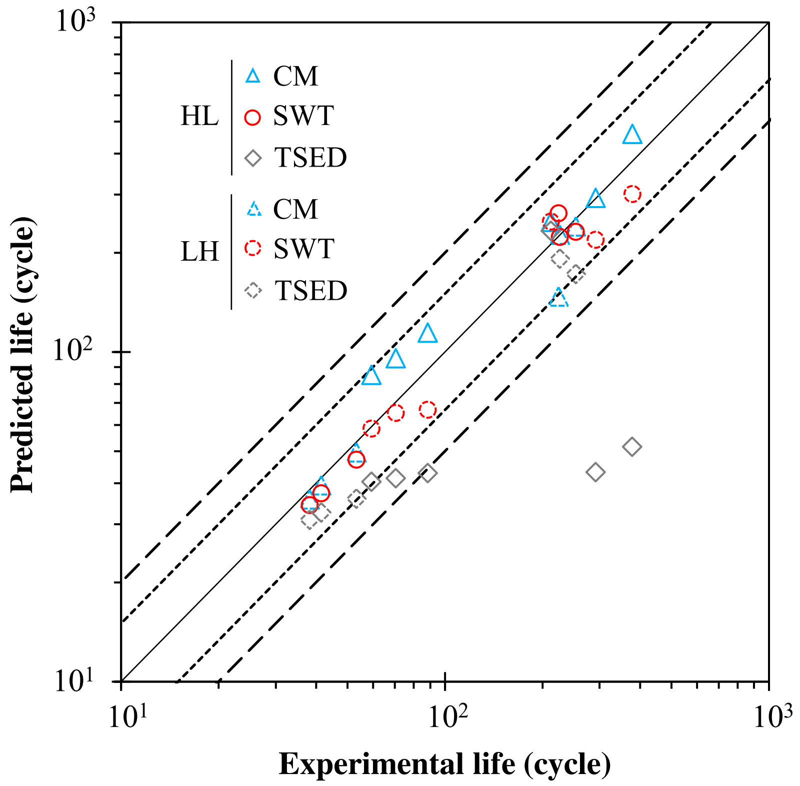

Figure 10. Comparison of the predicted fatigue lives and the observed fatigue lives for the loading sequence tests. Calculations were computed from the midhalf life hysteresis loops obtained experimentally. Thinner and thicker dashed lines represent scatter bands of factors of 1.5 and 2.0, respectively.

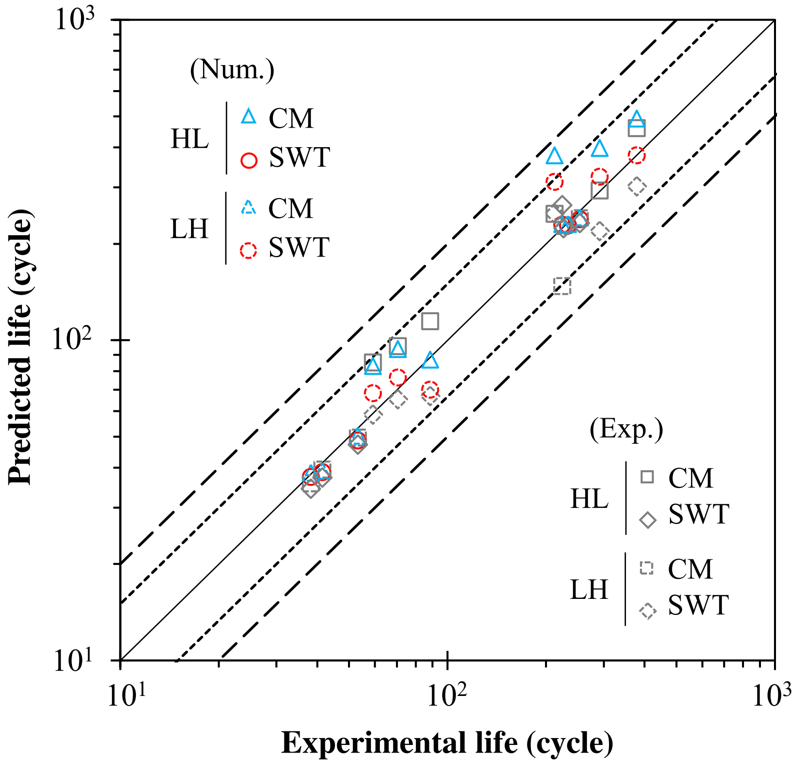

Figure 11. Comparison of the predicted fatigue lives and the observed fatigue lives for the loading sequence tests. Calculations were computed from the hysteresis loops simulated numerically. Thinner and thicker dashed lines represent scatter bands of factors of 1.5 and 2.0, respectively.

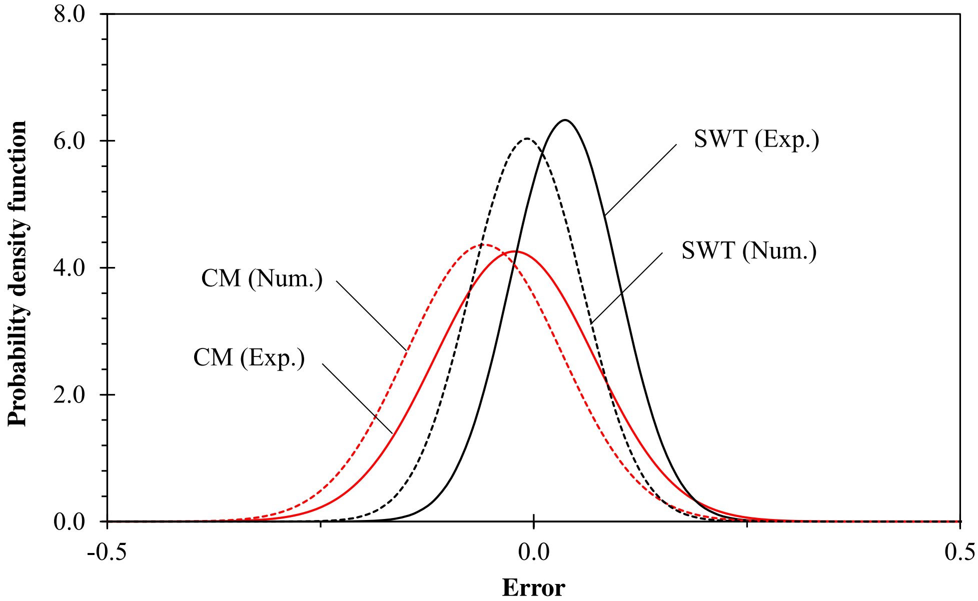

Figure 12. Probability density functions of the predictive error for the CM-based and SWT-based models. Full lines refer to the calculations carried out using the hysteresis loops collected in the experiments while the dashed lines refer to the calculations carried out using the hysteresis loops simulated numerically.